Title: THE HYDROPHOBIC MISMATCH DETERMINES THE MISCIBILITY OF CERAMIDES IN LIPID MONOLAYERS

Authors: Dupuy Fernando, Maggio Bruno

PII: S0009-3084(12)00078-3
DOI: doi:10.1016/j.chemphyslip.2012.06.008
Reference: CPL 4132

To appear in: *Chemistry and Physics of Lipids*

Received date: 24-4-2012
Revised date: 20-6-2012
Accepted date: 28-6-2012

Please cite this article as: Bruno, D.F.M., THE HYDROPHOBIC MISMATCH DETERMINES THE MISCIBILITY OF CERAMIDES IN LIPID MONOLAYERS, *Chemistry and Physics of Lipids* (2010), doi:10.1016/j.chemphyslip.2012.06.008

THE HYDROPHOBIC MISMATCH DETERMINES THE MISCIBILITY OF CERAMIDES IN LIPID MONOLAYERS

Dupuy, Fernando; Maggio, Bruno.*

Centro de Investigaciones en Química Biológica de Córdoba (CIQUIBIC, UNC–CONICET), Departamento de Química Biológica, Facultad de Ciencias Químicas, Universidad Nacional de Córdoba. Haya de la Torre y Medina Allende, Ciudad Universitaria, X5000HUA, Córdoba. República Argentina.

bmaggio@fcq.unc.edu.ar

* To whom correspondence should be addressed. Haya de la Torre y Medina Allende, Ciudad Universitaria, X5000HUA, Córdoba. República Argentina. Telephone: +54-351-5353855

Abstract

The organization of lipids within membranes strongly depends on the interaction with other lipid and protein molecules. Sphingolipids comprise a structurally diverse family, the ceramides being some of the simplest members. Although small chemical modifications of ceramide structure, such as varying the N-acyl chain length, lead to a complex polymorphism of this lipid, only long acyl chain ceramides have usually been studied and their properties became a putative hallmark for all ceramides. In this work, we studied the mixing behavior of C10:0 Cer, which has the N-acyl chain shorter than that of the sphingosine acyl chain and displays an expanded to condensed phase transition at 25 $mN.m^{-1}$ at 24 ºC, with ceramides N-acylated with longer fatty acyl chains C12:0, C14:0 and C18:0. The N-acyl chain length determined the miscibility of ceramides in Langmuir monolayers, as it was ascertained by the dependence of the mean molecular area, perpendicular dipole moment, surface topography and film thickness with the mixture composition. We found that, as the hydrophobic mismatch in ceramides increased complete miscibility, partial or complete immiscibility can occur.

Keywords

Ceramide monolayers, acyl chain length, mixing parameters, ideal behavior.

1. Introduction

Sphingolipids are important structural and physiological components of eukaryotic cell membranes. They are constituted by a long acyl chain aminediol base, usually C18 and C20 sphingosine, N-linked to a fatty acid. Ceramides are sphingolipids with the smallest polar head, with the hydroxyl groups of both C1 and C3 of the sphingosine base remaining unbound. In spite of this rather simple structure, ceramides can show a broad chemical diversity of the hydrocarbon moiety in terms of length asymmetry and unsaturation-hydroxylation degree in both the sphingosine base and the N-linked fatty acyl chain (Hannun and Obeid, 2011; Maggio et al., 2006; Maggio et al., 1986; Zheng et al., 2006). These lipids are present in the plasma and inner membranes of cells in relatively low amounts but can transiently increase as a response to signaling events (Futerman and Hannun, 2004; Kitatani et al., 2008). Among other signal transducing biological activities, a steep rise of up to 10% of C16 ceramide levels in the plasma membrane was reported as a consequence of sphingomyelinase activity and this was related to induction of apoptosis (Hannun, 1996). Also, ceramide represents a hub of paramount significance in the sphingolipid metabolism because it links the synthetic and degradative pathways of sphingomyelin, complex sphingolipids and active sphingosine derivatives (Hannun and Obeid, 2011; Kitatani et al., 2008; Zheng et al., 2006). On the other hand, ceramides with hydroxylated fatty acids and with very long hydrocarbon chains are main constituents of the stratum corneum of the skin (ten Grotenhuis et al., 1996) and sperm cells (Furland et al., 2007).

Long- and short-chain species of sphingolipids can be formed endogenously in cell membranes, or as a consequence of metabolism (Merrill, 2002; Ogretmen et al., 2002). Actually, the capacity of sphingomyelinase to degrade sphingomyelins with different N-acyl chain lengths to ceramides with the same hydrocarbon moieties, and the remodelling activity of transacylases can further extend the variety of N-acyl chain lengths in ceramides (Kitatani et al., 2008). In spite of such chemical diversity, most of the biological properties of ceramide continue to be interpreted almost exclusively on the base of the properties of the derivatives with N-acyl chain lengths of 16-20C that form solid phase domains in phospholipid bilayers. This is somehow paradoxical because many of the cellular effects ascribed to natural and long chain synthetic ceramides have been obtained with soluble analogs having a short N-acyl chain that are much less condensed (Dupuy et al., 2011; Sot et al., 2005). When dispersed in water, ceramides N-linked with fatty acids having more than 16C length display the highest melting temperature observed in membrane lipids (Maggio et al., 1986; Shah et al., 1995). However, even C16:0 Cer can exhibit a rich mesomorphic behavior in planar interfaces showing not only condensed (Löfgren and Pascher, 1977; Vaknin and Kelley, 2000) but also expanded states, as well as isothermal and isobaric expanded-condensed and condensed-condensed transitions (Fanani and Maggio, 2010).

In mixtures with phospholipids, the ordered phase domains formed by C16:0 Cer have been shown to exclude fluorescent probes that are markers of gel phases (Castro et al., 2007), to form solid patches inside gel phase domains (Silva et al., 2007; Staneva et al., 2009) and to induce other lipids, such as sphingomyelin, to become condensed or to transform to gel-type phase (Busto et al., 2009; Carrer et al., 2006; Castro et al., 2007). In Langmuir monolayers, the equilibrium compression modulus of C16:0 Cer was shown to be higher than that of saturated sphingomyelin (Busto et al., 2009; Catapano et al., 2011) and phosphatidylcholine, both in condensed phase, and that of lipid extracts from prokaryote sources (Espinosa et al., 2011). Also, even though plastic softening of C16:0 Cer was observed in dynamic compression experiments at high frequency of deformation, ceramide monolayers were stiffer and had higher viscosities compared to sphingomyelin (Catapano et al., 2011). On the other hand, the condensed domain size and morphology of Ceramides/PC mixtures and the degree of rigidity of the fluid phase outside solid domains varies when increasing the N-acyl chain length from 16 to 24C or in the presence of unsaturation (Pinto et al., 2011). Similar results in the morphology of the condensed domains were obtained in mixed monolayers of DMPC with ceramides having fatty acids with chain lengths from C2 to C24 (Holopainen et al., 2001; Karttunen et al., 2009). Also, we showed that besides being able to acquire highly ordered, solid like states, ceramide monolayers can display expanded to condensed phase transitions depending on the length of the N-linked saturated fatty acid from 10 to 16C (Dupuy et al., 2011). The fatty acyl chain length also determines the film dipole potential, domain morphology, surface topography, elasticity and optical thickness of the interface of ceramide monolayers (Dupuy et al., 2011).

In this work we explored the effect of variations of the length of the N-linked acyl chain on the mixing behavior between ceramides having the same sphingosine base. By maintaining invariant the polar head group region of the mixed interface, our intention was to get an insight on whether long chain saturated ceramides can interact with less ordered phases formed by shorter chain ceramides as they do with liquid-expanded phospholipids. Each mixture was evaluated by assessment of the compositional dependence of the mean molecular area, compressibility modulus and the phase transition surface pressure. The isotherms were further complemented with measurements of the dipole potential, calculation of the resultant dipole moment, imaging of the film topography and determination of the optical thickness by Brewster Angle Microscopy (BAM).

2.1 Materials and Methods

N-decanoyl-D-*erythro*-sphingosine (C10:0 Cer), *N*-lauroyl-D-*erythro*-sphingosine (C12:0 Cer), *N*-myristoyl-D-*erythro*-sphingosine (C14:0 Cer), *N*-palmitoyl-D-*erythro*-sphingosine (C16:0 Cer), *N*-stearoyl-D-*erythro*-sphingosine (C18:0 Cer) and *N*-lygnoceroyl-D-*erythro*-sphingosine (C24:0 Cer) were purchased from Avanti Polar Lipids Co. (Alabaster, AL. USA) and used without further purification. Ceramides were dissolved in chloroform: methanol (9:1) using HPLC grade solvents (Merck) at 1 nmol.μL^{-1} and stored at -72 °C until use in pyrex glass tubes (Corning) sealed with Teflon coated tapes. Mixtures were prepared by taking aliquots of the corresponding ceramide solutions with a Hamilton syringe.

The subphase for Langmuir monolayer experiments was 145 mM NaCl (Merck). Water was purified by successive passage through Elix10 and MilliQ Gradient A10 systems (Millipore), which yield a resistivity of 18.2 MΩ and organic content of 5 ppb. Besides, absence of surface-active impurities in the subphase solution and the spreading solvent were routinely checked as previously described (Perillo et al., 1993).

Lipid monolayers were obtained by spreading up to 10 nmol of ceramide onto the aqueous surface. Compression isotherms were carried out in a NIMA 102M system (KSV NIMA – Biolin Scientific) equipped with Delrin barriers, a Teflon trough with a surface area of 86 cm^2 and Wilhelmy paper sensor for surface pressure measurements. These isotherms were indistinguishable from those obtained with other equipment (KSV-Minitrough, Biolin Scientific; Monofilmeter, Mayer Feintechnik) using platinized Pt sensing plate. The surface potential of the films was simultaneously measured with an air-ionizing ^{241}Am electrode located 5 mm above the surface and a Ag/AgCl miniature (Cypress System) as a reference electrode in the subphase. The whole system was enclosed in an acrylic box surrounded by a metallic grid connected to ground, in order to reduce external interference in the measurements of surface potential. Films were compressed at 5 $Å^2.molec^{-1}.min^{-1}$, a twofold reduction of the compression rate did not cause changes in the isotherm features. The temperature was controlled within 0.2 ºC by means of an external circulating water bath (Haake F3C) connected to the Langmuir balance and a temperature sensor in the trough.

Imaging of the monolayers by Brewster Angle Microscopy (BAM) was carried out with an auto-nulling imaging ellipsometer (Nanofilm EP3sw Imaging Ellipsometer – Accurion GmbH, Germany) equipped with a 532 nm laser, 10X objective and CCD camera, which operates at a resolution of 2 μm in the BAM mode. By using p-polarized light, the equipment automatically finds the actual Brewster angle of the subphase by measuring the intensity of reflected light at several angles of incidence.

The measured p-polarized light reflectivity (Rp) is related to film thickness (l) (C. Lheveder, 2000) according to:

$$l=\frac{\sqrt{R_p}}{\sin\left(2\theta_B\text{-}90\right)}\cdot\frac{\lambda}{\pi}\cdot\frac{\left(n_1^2\text{-}n_2^2\right)}{\sqrt{n_1^2+n_2^2}}\cdot\frac{n^2}{\left(n_1^2\text{-}n^2\right)\left(n_2^2\text{-}n^2\right)}$$

Where n_1 is the refractive index of the air (n_1=1), n_2 is the refractive index of the subphase (typically 1.336), λ is the laser wavelength (5230 Å), n is the refractive index of the film (n=1.49)(Dupuy et al., 2011; Howland et al., 2007) and π is the Euclidean constant. The refractive index of the subphase was calculated from the measured Brewster angle (θ_B) according to:

$$\tan\theta_B=\frac{n_2}{n_1}$$

For 0.145 M NaCl, values of n_2 corresponded typically to 1.336. The public software ImageJ (1.43u Wayne Rasband – National Institutes of Health, USA) was used for gray level determination on the bare images obtained by BAM.

2.2 Analysis of isotherms

The surface pressure at which monolayer transitions between expanded and condensed phases occurred was calculated by means of the method of second and third derivative of π (surface pressure) with respect to A (mean molecular area) (Brockman et al., 1980).

The in-plane elasticity of the films was studied by determining the surface compressional modulus (C_S^{-1}) according to:

$$C_S^{-1}=\text{-}A\left(\frac{\partial\pi}{\partial A}\right)$$

where π is the surface pressure at the corresponding A (Gaines, 1966). The in-plane elasticity of the mixtures was compared with the calculated mean elasticity of ideally mixed films, taking into account the C_S^{-1} of the pure components, the mole fraction X_1 and X_2 and the mean molecular area A_1 and A_2 in the mixture at the corresponding π (Ali et al., 1994), according to:

$$\overline{C}_{S\,\pi}^{-1}=\left(X_1\left(\frac{C_{S1}^{-1}}{A_1}\right)_\pi+X_2\left(\frac{C_{S2}^{-1}}{A_2}\right)_\pi\right).\left(X_1.A_1+X_2.A_2\right)$$

The resultant dipole moment perpendicular to the interface ($\mu_\perp$) was calculated directly from surface potential-mean molecular area isotherms (Gaines, 1966; Smaby and Brockman, 1990) according to:

$$\mu_\perp = \frac{1}{37.7}.A.\Delta V$$

where ΔV is the surface potential of the monolayer in mV at the corresponding A in A^2.

The mean molecular area and the perpendicular dipole moment of the mixtures at the corresponding surface pressure π were compared with the values predicted from the additivity rule (Gaines, 1966) according to:

$$\bar{A}_\pi = x_1 (A_1)_\pi + x_2 (A_2)_\pi$$
$$\bar{\mu}_\pi = x_1 (\mu_1)_\pi + x_2 (\mu_2)_\pi$$

Where A_1, A_2 and μ_1, μ_2 are the mean molecular area and perpendicular dipole moment, respectively, of the component 1 and 2, respectively, at the surface pressure π. For the C12:0/C10:0 Cer mixture, where both components display expanded to condensed monolayer transition at the temperature at which the experiments were carried out, the ideal values of mean molecular areas were obtained from theoretical isotherms with an ideal transition surface pressure, calculated from the additivity of the transition surface pressures of the pure components.

3. Results

3.1 C12:0 Cer – C10:0 Cer

The compression isotherms (π-A) at 24 °C of monolayers of pure ceramides with fatty acyl chain lengths of 10 (C10:0 Cer) and 12 (C12:0 Cer) carbons displayed an expanded phase behavior at surface pressures below 25.6 and 4.9 $mN.m^{-1}$, respectively. By compressing the films above these surface pressure values, a first order transition in which the condensed phase nucleated into domains within the liquid-expanded phase was observed. Further compression takes C10:0 Cer and C12:0 Cer to the closest molecular packing state, producing condensed films which collapsed at a mean molecular area of ~40 A^2.

The pressure-area isotherms of films composed by different mole fractions of these two closely related lipids exhibited a highly cooperative two-dimensional transition from expanded-to-condensed states (Fig 1 A). The surface pressures at which this transition took place varied with the composition of each mixture, decreasing in approximately linear manner with increasing mole fractions of C12:0 Cer (see also Fig 2A).

The resultant perpendicular dipole moment reflected molecular rearrangements at the monolayer phase transition, as indicated by a steep decrease of the dipole moment at the surface transition pressure (Fig 1B, see arrows). Thus, the dependence of the phase transition surface pressure with film composition was independently confirmed by the variation of the perpendicular dipole moment with the surface pressure.

The variation of the in-plane elasticity with the surface pressure of the film also reflected clearly the monolayer phase transition of the mixed film and its dependence with composition (Fig 1C). The liquid-expanded phase of the mixtures showed similar values of surface compressibility modulus and a decrease at the corresponding transition surface pressure was observed (see arrows, Fig 1C).

At a surface pressure of 3 $mN.m^{-1}$, both C10:0 Cer and C12:0 are characterized by an expanded behavior. At this surface pressure, their mixtures showed no significant deviations from ideality of mean molecular area (Fig 3A) or the perpendicular dipole moment (Fig 3B) at any composition. Also, p-reflectivity at the Brewster angle showed the formation of homogeneous films (Fig 4A) with reflectivity levels (optical thickness) higher than for the pure C10 Cer (continuous line) and accounted for by a linear contribution of that of the pure components, weighted by their proportions in the mixture (see Fig 1D).

The surface compressional modulus of the mixed films also showed little positive deviations from the behavior expected for the ideally mixed pure components at a surface pressure of 3 $mN.m^{-1}$ and $X_{C12:0}$ >0.6 (Fig 3C).

At a surface pressure of 15 $mN.m^{-1}$, the mixtures showed no significant deviations in area from the additivity rule (Fig 3D) but a perpendicular dipole moment depolarization occurred, compared to the ideal behavior, at $X_{C12:0}$ below 0.5, (a decrease of ~40 mD at $X_{C12:0}$ = 0.4, Fig 3E). At these proportions of $X_{C12:0}$, and values of surface pressure, the mixtures are below the transition surface pressure and the surface compressional modulus corresponds to that of an expanded state (Fig 3F). Also, the p-reflectivity at the Brewster angle showed the presence of a homogeneous film (Fig 4B), even though pure C12:0 Cer is condensed at surface pressures of 15 $mN.m^{-1}$.

The reflectivity levels of the films at 15 $mN.m^{-1}$ were lower than those calculated by a weighted additivity of the values for pure components. Increasing the C12:0 Cer content above $X_{C12:0}$ = 0.4 takes the films into the condensed state, whereas the transition surface pressure of the mixtures is lowered due to the higher amount of C12:0 Cer (Fig 1A, 2A). At this surface pressure, mole fractions of C12:0 Cer above 0.5 lead to an increase of the perpendicular dipole moment of the films (Fig 3 E). BAM imaging of these films also showed phase coexistence during the transition that were characterized by the formation of discrete domains with reflectivity levels higher than the darker homogeneous expanded phase (Fig 4 E, H). As shown in Fig 2 B for the film composition of $X_{C12:0\ Cer}$= 0.4, the domain size increased significantly over a narrow range of surface pressure, in agreement with the observed monolayer phase transition of the π-A isotherms of C12/C10 mixtures. Interestingly, the aspect of the domains at the transition varied with film composition and evolved from small size and round to large flower-like shapes, as the content of C12:0 Cer in mixtures was increased (Fig 4 B, E, H, K). The measured reflectivity of the expanded and condensed phases was similar, within errors, to the values predicted by the ideal additive behavior of the pure components.

The surface compressibility of the mixed films at 15 $mN.m^{-1}$ showed negative deviations from the ideal additive behavior. The values of C_S^{-1} remained with no significant changes compared to the compressibility of C10:0 Cer as the mole fraction of C12:0 Cer increased up to ~0.4-0.5 (Fig 3F). Further increments of the amounts of C12:0 Cer in mixtures yielded non ideal films with increasing in-plane elasticity, but ideal behavior was not found.

At 32 $mN.m^{-1}$, all the C12:0/C10:0 Cers mixtures were in a condensed state. The mixtures showed again almost no deviation from the additivity rule of MMA over all the composition range (Fig 3 G) and a small surface depolarization of ~15mD at $0.2<X_{C12:0}<0.8$ (Fig 3 H). The in-plane elasticity of the mixed films decreased linearly with the increase of the mole fraction of

C12:0 Cer and showed minor negative deviations from the ideal behavior only at $X_{C12:0}$ <0.5 (Fig 3 I).

Visualization of the film topography by BAM of the condensed phase of the C10/C12 Cer mixtures showed poorly defined contours of the condensed domains with respect to the background (Fig 4 C,F,I,L). However, the difference in reflectivity between them was still within the instrument resolution.

3.2 C14:0 Cer – C10:0 Cer

In mixtures with C14:0 Cer, the surface pressure for the expanded-condensed transition of ceramide monolayers decreased from 25.9 at $X_{C14:0\ Cer}$ =0 to ~2 mN.m^{-1} at $X_{C14:0}$ = 0.5 (Fig 5A, 2A). Also, the cooperativity of the process decreased compared to the mixtures with C12:0 Cer as indicated by the much less horizontal surface pressure along the transition region of the isotherm at increasing C14:0 content. At $X_{C14:0\ Cer}$ > 0.5 a shoulder on the compression isotherm, at a surface pressure of 19 mN.m^{-1}, that did not change with further increase in $X_{C14:0}$ could be observed indicating a demixing of a C10:0 Cer enriched phase (see Inset at Fig 5A).

The perpendicular dipole moment also decreased at the surface pressure where monolayer phase transition was observed in the π-A isotherms (Fig 5B) but the decrease was not as steep as in the case of the more cooperative phase transition observed in C12/C10 Cer mixtures (compare Fig 5B and 1B). Nevertheless, the abrupt downward shift of the phase transition surface pressure also occurred in the mixed films with C14:0 Cer (Fig 2A).

The expanded-condensed transition determined by the π-A derivative method could also be easily detected in C_S^{-1} *vs* surface pressure plots because the surface compressibility modulus dropped at the transition surface pressure (Fig 5C). Also, below the transition surface pressure, the elasticity of mixtures was significantly lower than that of C14:0 Cer and behaved much more like that of C10:0 Cer, indicating the formation of a liquid expanded state.

At 5 mN.m^{-1}, the mixtures showed no significant MMA deviation over the whole compositional range (Fig 6A). However, at 0.2<$X_{C14:0\ Cer}$<0.8, the films were slightly depolarized (Fig 6B) with respect to the ideal mixing prediction. At $X_{C14:0}$ < 0.4 a homogeneous film (see Fig 7A further below), with higher levels of reflectivity at the Brewster angle (optical thickness) compared to the expanded phase of C10:0 Cer was observed. This suggests the presence of C14:0 Cer in the expanded phase (Fig 5D), although the pure lipid forms condensed films at all surface pressures at 24 °C.

At $X_{C14:0\ Cer}$>0.5, the transition surface pressure dropped below 1 mN.m^{-1} (Fig 2A) and could no longer be detected. Condensed-expanded phase coexistence was detected by BAM, even at full

separation of the mobile barriers (null surface pressure, ie, 0 $mN.m^{-1}$). The condensed phase occurred in polymorphic domains, with rather elongated stripes coexisting with rounded shapes (Fig 7 G, J). Also, the reflectivity levels of the expanded phase was higher than for C10:0 Cer, whereas the measured reflectivity of the condensed phase of the mixed film was lower than that of C14:0 Cer.

The surface compressional modulus of the mixtures at 5 $mN.m^{-1}$ also showed negative deviations from the ideal behavior (Fig 6C). At $X_{C14:0\ Cer} < 0.5$, the in-plane elasticity remained similar to the values of C10:0 Cer. However, at higher proportions of C14:0 Cer, the C_S^{-1} of the mixtures increased but without reaching the ideal values calculated from the elasticities of the pure components (Fig 6C).

At 10 and 15 $mN.m^{-1}$, small negative deviations of MMA (Fig 6D) and ~20mD decrease of the surface dipole moment were observed for films containing $0.2 < X_{C14:0} < 0.8$ (Fig 6E). At $X_{C14:0} = 0.2$, the isotherm of the mixture showed an expanded-condensed transition at 18 $mN.m^{-1}$ which was also evidenced by BAM as a nucleation of round-shape condensed domains within the continuous expanded phase (not shown). At $X_{C14:0} = 0.4$, a monolayer phase transition was observed at a surface pressure of ~4.7 $mN.m^{-1}$ (Fig 5A). At this surface pressure, BAM measurements indicated nucleation of condensed phase domains within the homogenous expanded phase (Fig 7D). Different to films with lower content of C14:0 Cer, the domains at $X_{C14:0} = 0.4$ that are formed upon compression displayed flower-like shapes (Figs 7D, E) and higher reflectivity levels, suggesting a higher content of C14:0 Cer in the growing phase. The domain growth in $X_{C14:0}$ Cer =0.4 films encompassed a rather wide range of surface pressures, from ~4.7 to almost 25 $mN.m^{-1}$ (Fig 2B), as a consequence of the poor cooperativity of the monolayer phase transition. The surface compressibility of the mixtures at 15 $mN.m^{-1}$ showed negative deviations compared to the ideal behavior (Fig 6F) that were even higher than those occurring at 5 $mN.m^{-1}$. In the proportions $0<X_{C14:0\ Cer}<0.5$, the compressibility of the films remained similar to those of pure C10:0 Cer values. At higher contents of C14:0 Cer, the in-plane elasticity of the mixed films increased, but without reaching the predicted ideal values for C_S^{-1} (Fig 6 F).

At surface pressures above 30 $mN.m^{-1}$, both MMA (Fig 6G) and perpendicular dipole moment (Fig 6H) showed no significant deviation from the ideal behavior. At this surface pressure, both pure components are in a condensed phase state. The topography of the mixed films exhibited surface heterogeneity (Fig 7C, F, I, L). At $X_{C14:0} > 0.4$, the condensed domains that were formed during compression did not cover the whole surface. Instead, the remaining expanded film formed a condensed phase of its own at a surface pressure of ~ 20 $mN.m^{-1}$ and with a reflectivity level lower than that of the domains that nucleated at ~4.7 $mN.m^{-1}$ (Fig 7F). Thus,

the new condensed phase remained separate from the former one, yielding a fully condensed phase-separated film. At increasing proportions of C14:0 Cer ($X_{C14:0}$ >0.5) a similar behavior was observed. The condensed domains that were already present a zero surface pressure did not mix with the continuous phase when the latter transformed into a condensed state at ~19 mN.m^{-1}, yielding a film with heterogeneous surface (Fig 7I, L), and with high surface compressional modulus (Fig 6I). Different to the surface compressibility of the mixtures at 5 and 15 mN.m^{-1}, the in-plane elasticity at 32 mN.m^{-1} did not show significant deviations from the ideal behavior (Fig 6I).

3.3 C18:0 Cer C10:Cer

Compression isotherms of the mixtures of C18:0 Cer/C10:0 Cer with increasing proportions of $X_{C18:0\ Cer}$ displayed a shift of the expanded state towards lower values of MMA. However, the expanded-condensed transition was still observed at ~19 mN.m^{-1} and displayed no significant changes over the mole fractions $0.1<X_{C18:0\ Cer}<0.9$ (Fig 2A), indicating that a C10:0 Cer enriched expanded phase did not mix with of C18:0 Cer (Fig 8A). Mixtures of ceramides with even longer saturated chain rendered essentially the same behavior. In the case of C24:0 Cer, increasing proportions of this long chain ceramide in the mixtures produced no modification of the expanded-condensed transition at 25 mN.m^{-1} of C10:0 Cer in any composition of the assessed mixtures (data not shown).

The perpendicular dipole moment decreased at the surface pressure of the monolayer phase transition (Fig 8B). Also, the surface compressional modulus of the mixed films showed a steep decrease at the same surface pressure of the transition (Fig 8C)

The mixed films showed no significant deviations of MMA from ideality either at 5 (Fig 9A) and at 15 mN.m^{-1} (Fig 9D) at any composition. The molecular dipole moment, on the other hand, decreased ~15 mD at 15 (Fig 9E) and at 20 mN.m^{-1} at $0.1<X_{C18:0}<0.9$.

The surface compressional modulus of the films at 5 (Fig 9C) and 15mN.m^{-1} (Fig 9F) linearly increased with low slope when the mole fraction of C18:0 Cer in the mixed films increased from 0 to 0.5. At higher proportions of C18:0 Cer, C_S^{-1} increased with a steeper slope. However, when compared to the ideal behavior, the compressibility of the films at $X_{C18:0\ Cer} < 0.9$ exhibited negative deviations, except at 32 mN.m^{-1}.

The film topography as revealed by BAM showed expanded-condensed phase coexistence even at surface pressure of 0 mN.m^{-1} (not shown) over the whole range of composition of the mixed films of C18:0 Cer/C10:0 Cer. At $X_{C18:0\ Cer} = 0.2$, condensed domains were mostly round shaped (Fig 10A, B), with a mean surface area that did not increase upon film compression (Fig 2B). Also, the expanded phase displayed reflectivity levels similar to that of the expanded phase of

C10:0 Cer while the levels of reflectivity of the condensed domains were similar to those of C18:0 Cer, suggesting that both molecules formed separate phases (Fig 8D). At higher $X_{C18:0\ Cer}$, condensed domains showed coexistence of rounded and relatively long striped shapes (Fig 10D, E), or only a striped phase that coalesced upon film compression (Fig 10G, H, J, K). The size of the rounded domains in films with $X_{C18:0\ Cer} = 0.4$ did not increase with the surface pressure (Fig 2B). The condensed domains observed in C18:0/C10:0 Cer mixtures were smaller compared to condensed domains in mixtures of C14:0/C10:0 Cers, which is in agreement with the higher internal repulsion of the condensed domains formed by C18:0 Cer mixtures, as a consequence of the longer acyl chain and higher dipole moment molecule of C18:0 Cer compared to C14:0 Cer.

At 32 $mN.m^{-1}$ the measured MMA of the mixtures did not show significant deviations from the ideal behavior over the whole compositional range (Fig 9G). However, a decrease of the perpendicular dipole moment of the mixtures was observed, with a maximal negative deviation of 30mD at $X_{C18:0} = 0.3$ (Fig 9H). The surface compressibility modulus of the mixtures at 32 $mN.m^{-1}$ did not show significant deviations compared to ideal behavior (Fig 9I).

At pressures near the expanded-condensed transition (ie ~20 $mN.m^{-1}$), the reflectivity levels of the expanded phase changed to values similar to those of the condensed phase of C10:0 Cer (Fig 8C). However, at 32 $mN.m^{-1}$, the condensed phases do not mix but remained separate, giving rise to a condensed film with heterogeneous surface, and the C10:0 Cer enriched phase nucleated around the condensed (C18:0 Cer enriched) domains (Fig 10C, F, I, L).

According to the collected data, the difference in the N-linked acyl chain length of ceramides markedly determines their mixing behavior. Even though ceramides with fatty acyl chain lengths longer than 14C lead to films with similar compression isotherms and surface elasticity, C14:0 and C16:0 Cers were able to form expanded mixed films with C10:0 Cer whereas in the condensed state a heterogeneous film is formed. On the other hand, C18:0 and C24:0 Cer, owing to their longer N-acyl chain length with respect to C10:0 Cer, did not mix either in the expanded nor in the condensed state.

In order to assess further this behavior, we compared the mixing properties of two mixtures with identical acyl chain length mismatch: C16:0 Cer - C12:0 Cer at 40 °C and C14:0 Cer –C10:0 Cer at 23 °C (the latter was discussed above). As can be seen in Fig 11, the surface pressure of the expanded-condensed monolayer transition of C12:0 Cer decreased at increasing proportions of C16:0 Cer in the mixture, indicating that the expanded phase became enriched with the longer acyl chain ceramide, even though C16:0 Cer does not form expanded phases by itself except at temperatures higher than 48 ºC (Fig 11, inset). Interestingly, compression isotherms of C16:0 Cer/C12:0 Cer and C14:0 Cer/C10:0 Cer are remarkably similar (see Fig 11 and Fig 5A),

pointing out that the hydrophobic chain mismatch appears to be a very important determinant for the two-dimensional miscibility of ceramides with saturated N-acyl chains.

4. Discussion

Biological membranes are complex polymorphic mixtures of proteins and a large variety of lipids, which makes rather difficult the comprehension in simple molecular terms of the structural dynamics of their lateral organization. For this reason, most of what we actually know about the organization of biomembranes has derived from the study of the properties of single components or of some simple mixtures in model systems that allow proper control of the surface parameters.

Ceramides are the most simple sphingolipids and those with long saturated acyl chains exhibit strong intermolecular association which allow optimal packing, whereby van der Waals interactions between hydrocarbon chains and hydrogen bonding in the polar head region are optimized (Boggs, 1987; Löfgren and Pascher, 1977), leading to high bulk transition temperatures (Maggio et al., 1986; Shah et al., 1995; Sot et al., 2005). As a consequence, such ceramides form segregated solid-like condensed domains, both in bilayers and monolayers that even exclude fluorescent probes and proteins (Busto et al., 2009; Carrer and Maggio, 1999; Castro et al., 2007; Chiantia et al., 2008; Holopainen et al., 2001; Karttunen et al., 2009; Lopez-Montero et al., 2010). This has somehow introduced the bias that *all* ceramides would be condensed-type of compounds forming solid-like domains at all degrees of surface density. However, ceramides with N-acyl chain length shorter than the hydrocarbon moiety of sphingosine can form expanded phases and undergo typical monolayer liquid-expanded to condensed transitions at defined surface pressures at room temperature (Dupuy et al., 2011). The expanded to condensed transition surface pressure was strongly affected by the length of the acyl chain, showing an increase of ~20mN.m^{-1} when two methylene groups of C12:0 Cer (π_T = 4.9 mN.m^{-1} at 24 °C) are removed from the N-linked fatty acid to yield C10:0 Cer (π_T= 25.6 mN.m^{-1}).

As shown in this work, the strong influence of the properties of the N-linked fatty acid acyl chain is also reflected in the behavior of C10:0 Cer mixed with ceramides of increasing acyl chain length. The mixtures of C10:0 – C12:0 Cer showed ideal mixing, even though their minimal mismatch in fatty acid acyl chain length resulted in a considerable difference in the tendency to adopt the condensed state, as shown above by the variation of the transition surface pressure with the composition of the mixed films. The linear decrease of the transition surface pressure with the increasing proportions of C12:0 Cer indicates ideal mixing. Also, the surface topography, as revealed by BAM is in keeping with this behavior, and shows that homogeneous films are formed over the whole range of composition, both in the expanded and in the condensed states.

It is worth mentioning that in the phase transition region of each mixture, condensed domain shape evolves from small and rounded C10:0 Cer-like domains in films with high proportions of this ceramide, to large flower-like domains similar to those of C12:0 Cer in films enriched in the latter lipid. The population of condensed domains observed during the monolayer phase transition and the narrow range of surface pressure over which domain formation took place also supports that the behavior of the mixture resembled that of a single molecular entity that cooperatively transforms from an expanded to a condensed state. In this way, a broad spectrum of film elasticity in different states of molecular packing is obtained when the monolayer composition and surface pressure of this mixture is modified.

Increasing the N-linked acyl chain length of ceramide to 14C gave rise to condensed films at temperatures below 35 °C (Fig 11, Inset). However, when studied at 24 °C, C14:0 Cer was able to form mixed expanded phases with C10:0 Cer. This is indicated by the dependence with composition of the decrease of the transition surface pressure with increasing proportions of C14:0 Cer, which reached null values when the content of C14:0 Cer is above 50 mole percent. At these compositions, partial demixing of the components was indicated by the appearance of a poorly defined shoulder at 19 $mN.m^{-1}$ in the π-A isotherm of the mixed films, a surface pressure that is close to that causing the liquid expanded-condensed transition of pure C10:0 Cer. In addition, BAM studies confirmed this behavior: at low C14:0 Cer content (<40%) and below the transition surface pressure of the film, the mixtures formed expanded films that appeared homogeneous (no evidence of phase separation, at least within BAM resolution) and thicker than the expanded phase formed by C10:0 Cer. Compressing the films beyond the LE boundary, condensed domains nucleated at a surface pressure corresponding to the monolayer phase transition, indicated by the inflexion point in the π-A isotherm and the domain size increased as the available area was further reduced. The phase transition region of the C14:0/C10:0 Cer mixtures was markedly non-horizontal and the expanded/condensed phase coexistence during the condensed domains growth took place in a wide range of surface pressure. In the case of $X_{C14:0\ Cer} = 0.4$ mixture, the first domains nucleated at 5 $mN.m^{-1}$ (at MMA of 63 A^2) but reached their maximum size at a surface pressure of 25 $mN.m^{-1}$ (MMA of 43 A^2), when the whole film acquired a condensed state with a surface compressibility modulus higher than 100 $mN.m^{-1}$. It is worth noting the condensed domains shape were flower –like, usually seen in Diffusion Limited Aggregation (DLA) processes, which implies domain growth by accretion of material dissolved in the film. This confirm that, when interacting with C10:0 Cer, C14:0 Cer adopt an expanded state and is able to diffuse to the nuclei of the growing solid phase (Aharony, 1996; Gutierrez-Campos et al., 2010).

However, at high surface pressures, the components were only partially mixed and coexistence of condensed phases is observed by BAM: a C14:0 Cer enriched phase that formerly nucleated

in domains and a continuous C10:0 Cer enriched phase that undergoes the expanded-condensed transition at surface pressures close to the transition pressure of C10:0 Cer. The partial miscibility of C10:0 Cer with C14:0 Cer that produces a C10:0 Cer enriched phase could explain the non-horizontal phase coexistence region of the π-A isotherm of the mixtures with $X_{C14:0\ Cer}$ <0. Arriaga *et al* have postulated that delayed domain growth yields a non zero rigidity at the phase coexistence region during film compression (Arriaga et al., 2010). The resistance imposed by the film to change the phase would be a consequence of the energy necessary for nucleation of new domains and the line tension and fluidity of the film where the condensed phase is formed that oppose domain growth. In the C14:0/C10:0 Cer mixture, the presence of the longer N-acyl chain length in the expanded phase increase the rigidity, which would also contribute to the increase of the surface pressure during phase coexistence.

Ceramides with N-linked acyl chains longer than 18 carbons produced condensed films that, different to C14:0 Cer, gave rise to phase coexistence when mixed with C10:0 Cer both at low and high surface pressures over the whole range of composition. Even though the small depolarization of the interface observed at 15 $mN.m^{-1}$ and 32 $mN.m^{-1}$ would suggest some molecular interactions between the components (although this could also arise from slight changes of surface hydration), the invariance of the transition surface pressure with the film composition and the similarity of the optical thickness of the expanded phase and condensed domains with C10:0 Cer and C18:0 Cer, respectively, at 15 $mN.m^{-1}$, indicate almost complete immiscibility. The topography of the mixtures visualized by BAM confirmed the phase separation at low and high surface pressures. At low surface pressure, C18:0 Cer enriched condensed domains were surrounded by a C10:0 Cer enriched expanded phase and showed smaller rounded or thinner striped shapes when compared to condensed domains observed in the mixtures of C14:0 Cer/ C10:0 Cer.

The effect of hydrophobic mismatch on the mixing of ceramides was studied by comparing the surface behavior of the pairs C14:0 Cer/C10:0 Cer at 23 °C and C16:0/C12:0 Cer at 40 °C. Both systems possess the same hydrocarbon chain length difference between the components, but enhanced van der Waals interactions would be expected for the longer acyl chain C16:0/C12:0 Cer mixture. However, the mixtures displayed identical behavior when force-area curves were compared, showing similar dependence (decrease) of the transition surface pressure with variations of the film composition, indicating the mixing of ceramides in the expanded state. Thus, N-acyl chain length determines both phase and mixing behavior of ceramide monolayers.

In previous studies in phospholipid bilayers, the hydrophobic mismatch between the components in binary mixtures induced different types of phase diagrams (Almeida et al., 2005; Mabrey and Sturtevant, 1976). For phosphatidylcholines, a difference of 6 carbons in the acyl

chain length in the mixture DLPC/DSPC produced a rather flattened fluid-gel coexistence line (Mabrey and Sturtevant, 1976; Risbo et al., 1995). In our monolayers studies of ceramides N-acylated with saturated fatty acids, 8 carbons in the N-acyl chain length mismatch was necessary to yield a similar mixing behavior of a solid/gel phase in equilibrium with a fluid liquid expanded/liquid crystalline one. On the other hand, both in phosphatidylcholine bilayers and ceramide monolayes, a hydrophobic mismatch of only 2 carbons (DMPC/DPPC and C12:0Cer/C10:0 Cer) produced mixtures with almost ideal mixing behavior (Mabrey and Sturtevant, 1976). A correlation in the mixing behavior in bilayers and monolayers was also observed for a hydrophobic mismatch of 4 carbons in both systems, a fluid phase composed by both components of the mixture and a ordered phase in coexistence with the fluid phase in a broad range of temperature/surface pressure (for the bilayer and monolayer experiments, respectively).

The presence of ceramide in the fluid state of the membrane was previously suggested by an increase of the fluorescence anisotropy of probes (Castro et al., 2007) and of the order parameter profile calculated by NMR (Hsueh et al., 2002) in experiments performed in mixtures with phospholipids in bilayer model systems. In our work we observed that, under conditions in which homogeneous expanded films of mixtures of a long and a short chain ceramide (C14:0/C10:0; C16:0/C12:0) are formed, no difference was found in the surface compressibility modulus compared to that of the expanded phase of the pure short chain ceramide. Actually, at 15 mN.m^{-1} the C_S^{-1} remains invariant with composition at $X_{C14:0\ Cer}$ <0.5, indicating that the elasticity of the whole film in this compositional range is accounted for the continuous expanded phase. On the other hand, BAM imaging showed that the expanded phase of the film was homogeneous at the micrometric level, and with p-reflectivity values higher than those of C10:0 Cer at the same surface pressure. This pointed out that the expanded state is actually composed both by C10:0 Cer and the thicker C14:0 Cer. At $X_{C14:0\ Cer}$ above 0.5, the excess of the long chain ceramide and the condensed domains lead to an increase of the surface compressional modulus and, consequently, higher amounts of condensed phase in the mixture (Fig 12B). In this manner, the elastic properties of the film do not change under the incorporation of a more solid state-prone lipid such as C14:0 Cer and, as long as the expanded phase is able to accommodate the molecules, no phase separation occurs.

In the C18:0 Cer/C10:0 Cer mixture, the behavior of the surface compressional modulus again reflects the effect of the condensed domains on the film elasticity. As described above, phase separation was observed in this mixture both at low and high surface pressure. C_S^{-1} of the mixtures was observed to increase with the content of C18:0 in the films, although with lower values than those predicted by the additivity rule (Fig 9C, F). This can be ascertained when comparing both the film in-plane elasticity and the optical thickness of the mixtures C18/C10

and C14/C10 ceramides, as a function of the composition (Fig 12B). The steady increase in C_S^{-1} of the whole film with increasing content of C18:0 Cer and the diminished optical thickness of the expanded phase in the mixture C18:0/C10:0 compared to the mixed film C14:0/C10:0 (Fig 12A) indicate that the surface properties of the film are not affected by the presence of a solid state-prone lipid when all the components are able to form a homogeneous expanded monolayer. At the point when the expanded phase becomes saturated with the long chain ceramide and condensed domains are formed, the whole film increases its average surface elasticity as the proportion of condensed phase is higher.

However, as the compressibility modulus value, both in the C18:0/C10:0 Cer and in the C14:0/C10:0 Cer mixture, are closer to that of the expanded continuous phase than to that of the condensed phase, the surface elasticity of films with expanded/condensed phase coexistence appears to behave according to the "plum-cake" model proposed for DPPC films in the phase coexistence region (Arriaga et al., 2010). In this model, the condensed domains in equilibrium with the expanded phase impose dynamic rigidity or stiffening upon compression but retain a global fluidity typical of expanded phases. In this manner, the increased amount of domains in the C18:0/C10:0 Cer as compared to C14:0/C10:0 mixture can also explain the higher values of the compressibility modulus by imposing more resistance to compression.

Thus, the capability of even a single type of ceramide to induce formation of solid-like segregated domains, with effects on the more liquid-like regions of membranes, should be considered only by strictly defining the type of N-linked acyl chain composition of the ceramides involved and how the components mix among themselves. Actually, one of the most commonly found ceramides in biological systems, C16:0 Cer, is not completely solid, different to what is usually conceived but it displayes a rich phase coexistence(Fanani and Maggio, 2010) even at physiological temperatures; with shorter chain expanded lipids it can also form expanded mixed phases depending on the surface pressure. It is worth recalling that the average lateral surface pressure largely fluctuates depending on the film compressibility, especially when phase coexistence occurs (Phillips et al., 1975). Thus, transient mixing-demixing processes among different ceramides species can occur in biomembranes, both inside ceramide-enriched rigid domains or platforms as well as in the expanded phase which can regulate lateral partitioning of lipids and proteins. The results described point out the rich complexity of mixing-demixing phenomena involving ceramides which should be taken into account when considering structure-mediated signaling in biomembranes (van Blitterswijk et al., 2003).

5. Acknowledgements.

This work was supported by CONICET, FONCYT (Grants BID-PAE 22642 and BID-PICT 1381) and SECyT-UNC, Argentina. F.D. is a postdoctoral fellow of CONICET and B.M. is a Career Investigator of CONICET.

6. Reference list.

Aharony, A., 1996. Fractal Growth, In: Bunde, A., Havlin, S. (Eds.), Fractals and Disordered Systems, Second ed. Springer-Verlag Berlin Heidelberg, New York.

Ali, S., Smaby, J.M., Brockman, H.L., Brown, R.E., 1994. Cholesterol's interfacial interactions with galactosylceramides. Biochemistry 33, 2900-2906.

Almeida, P.F., Pokorny, A., Hinderliter, A., 2005. Thermodynamics of membrane domains. Biochim Biophys Acta 1720, 1-13.

Arriaga, L.R., Lopez-Montero, I., Ignes-Mullol, J., Monroy, F., 2010. Domain-growth kinetic origin of nonhorizontal phase coexistence plateaux in langmuir monolayers: compression rigidity of a Raft-like lipid distribution. J Phys Chem B 114, 4509-4520.

Boggs, J.M., 1987. Lipid intermolecular hydrogen bonding: influence on structural organization and membrane function. Biochim Biophys Acta 906, 353-404.

Brockman, H.L., Jones, C.M., Schwebke, C.J., Smaby, J.M., Jarvis, D.E., 1980. Application of a microcomputer-controlled film balance system to collection and analysis of data from mixed monolayers. Journal of Colloid and Interface Science 78, 502-512.

Busto, J.V., Fanani, M.L., De Tullio, L., Sot, J., Maggio, B., Goni, F.M., Alonso, A., 2009. Coexistence of immiscible mixtures of palmitoylsphingomyelin and palmitoylceramide in monolayers and bilayers. Biophys J 97, 2717-2726.

C. Lheveder, S.H., and J Meunier, 2000. Brewster Angle Microscopy, In: Norde, W., Baszkin, A. (Eds.), Physical Chemistry of Biological Interfaces. Marcel Dekker, New York.

Carrer, D.C., Maggio, B., 1999. Phase behavior and molecular interactions in mixtures of ceramide with dipalmitoylphosphatidylcholine. J Lipid Res 40, 1978-1989.

Carrer, D.C., Schreier, S., Patrito, M., Maggio, B., 2006. Effects of a short-chain ceramide on bilayer domain formation, thickness, and chain mobililty: DMPC and asymmetric ceramide mixtures. Biophys J 90, 2394-2403.

Castro, B.M., de Almeida, R.F., Silva, L.C., Fedorov, A., Prieto, M., 2007. Formation of ceramide/sphingomyelin gel domains in the presence of an unsaturated phospholipid: a quantitative multiprobe approach. Biophys J 93, 1639-1650.

Catapano, E.R., Arriaga, L.R., Espinosa, G., Monroy, F., Langevin, D., Lopez-Montero, I., 2011. Solid character of membrane ceramides: a surface rheology study of their mixtures with sphingomyelin. Biophys J 101, 2721-2730.

Chiantia, S., Ries, J., Chwastek, G., Carrer, D., Li, Z., Bittman, R., Schwille, P., 2008. Role of ceramide in membrane protein organization investigated by combined AFM and FCS. Biochim Biophys Acta 1778, 1356-1364.

Dupuy, F., Fanani, M.L., Maggio, B., 2011. Ceramide N-acyl chain length: a determinant of bidimensional transitions, condensed domain morphology, and interfacial thickness. Langmuir 27, 3783-3791.

Espinosa, G., Lopez-Montero, I., Monroy, F., Langevin, D., 2011. Shear rheology of lipid monolayers and insights on membrane fluidity. Proc Natl Acad Sci U S A 108, 6008-6013.

Fanani, M.L., Maggio, B., 2010. Phase state and surface topography of palmitoyl-ceramide monolayers. Chem Phys Lipids 163, 594-600.

Furland, N.E., Oresti, G.M., Antollini, S.S., Venturino, A., Maldonado, E.N., Aveldano, M.I., 2007. Very long-chain polyunsaturated fatty acids are the major acyl groups of sphingomyelins and ceramides in the head of mammalian spermatozoa. J Biol Chem 282, 18151-18161.

Futerman, A.H., Hannun, Y.A., 2004. The complex life of simple sphingolipids. EMBO Rep 5, 777-782.

Gaines, G., 1966. Insoluble monolayers at liquid-air interfaces. Interscience Publishers, John Wiley & Sons, New York.

Gutierrez-Campos, A., Diaz-Leines, G., Castillo, R., 2010. Domain growth, pattern formation, and morphology transitions in Langmuir monolayers. A new growth instability. J Phys Chem B 114, 5034-5046.

Hannun, Y.A., 1996. Functions of ceramide in coordinating cellular responses to stress. Science 274, 1855-1859.

Hannun, Y.A., Obeid, L.M., 2011. Many ceramides. J Biol Chem 286, 27855-27862.

Holopainen, J.M., Brockman, H.L., Brown, R.E., Kinnunen, P.K., 2001. Interfacial interactions of ceramide with dimyristoylphosphatidylcholine: impact of the N-acyl chain. Biophys J 80, 765-775.

Howland, M.C., Szmodis, A.W., Sanii, B., Parikh, A.N., 2007. Characterization of physical properties of supported phospholipid membranes using imaging ellipsometry at optical wavelengths. Biophys J 92, 1306-1317.

Hsueh, Y.W., Giles, R., Kitson, N., Thewalt, J., 2002. The effect of ceramide on phosphatidylcholine membranes: a deuterium NMR study. Biophys J 82, 3089-3095.

Karttunen, M., Haataja, M.P., Saily, M., Vattulainen, I., Holopainen, J.M., 2009. Lipid domain morphologies in phosphatidylcholine-ceramide monolayers. Langmuir 25, 4595-4600.

Kitatani, K., Idkowiak-Baldys, J., Hannun, Y.A., 2008. The sphingolipid salvage pathway in ceramide metabolism and signaling. Cell Signal 20, 1010-1018.

Löfgren, H., Pascher, I., 1977. Molecular arrangements of sphingolipids. The monolayer behaviour of ceramides. Chemistry and Physics of Lipids 20, 273-284.

Lopez-Montero, I., Monroy, F., Velez, M., Devaux, P.F., 2010. Ceramide: from lateral segregation to mechanical stress. Biochim Biophys Acta 1798, 1348-1356.

Mabrey, S., Sturtevant, J.M., 1976. Investigation of phase transitions of lipids and lipid mixtures by sensitivity differential scanning calorimetry. Proc Natl Acad Sci U S A 73, 3862-3866.

Maggio, B., Fanani, M.L., Rosetti, C.M., Wilke, N., 2006. Biophysics of sphingolipids II. Glycosphingolipids: an assortment of multiple structural information transducers at the membrane surface. Biochim Biophys Acta 1758, 1922-1944.

Maggio, B., Fidelio, G.D., Cumar, F.A., Yu, R.K., 1986. Molecular interactions and thermotropic behavior of glycosphingolipids in model membrane systems. Chem Phys Lipids 42, 49-63.

Merrill, A.H., Jr., 2002. De novo sphingolipid biosynthesis: a necessary, but dangerous, pathway. J Biol Chem 277, 25843-25846.

Ogretmen, B., Pettus, B.J., Rossi, M.J., Wood, R., Usta, J., Szulc, Z., Bielawska, A., Obeid, L.M., Hannun, Y.A., 2002. Biochemical mechanisms of the generation of endogenous long chain ceramide in response to exogenous short chain ceramide in the A549 human lung adenocarcinoma cell line. Role for endogenous ceramide in mediating the action of exogenous ceramide. J Biol Chem 277, 12960-12969.

Perillo, M.A., Polo, A., Guidotti, A., Costa, E., Maggio, B., 1993. Molecular parameters of semisynthetic derivatives of gangliosides and sphingosine in monolayers at the air-water interface. Chem Phys Lipids 65, 225-238.

Phillips, M.C., Graham, D.E., Hauser, H., 1975. Lateral compressibility and penetration into phospholipid monolayers and bilayer membranes. Nature 254, 154-156.

Pinto, S.N., Silva, L.C., Futerman, A.H., Prieto, M., 2011. Effect of ceramide structure on membrane biophysical properties: the role of acyl chain length and unsaturation. Biochim Biophys Acta 1808, 2753-2760.

Risbo, J., Sperotto, M.M., Mouritsen, O.G., 1995. Theory of phase equilibria and critical mixing points in binary lipid bilayers. The Journal of Chemical Physics 103, 3643-3656.

Shah, J., Atienza, J.M., Duclos, R.I., Jr., Rawlings, A.V., Dong, Z., Shipley, G.G., 1995. Structural and thermotropic properties of synthetic C16:0 (palmitoyl) ceramide: effect of hydration. J Lipid Res 36, 1936-1944.

Silva, L.C., de Almeida, R.F., Castro, B.M., Fedorov, A., Prieto, M., 2007. Ceramide-domain formation and collapse in lipid rafts: membrane reorganization by an apoptotic lipid. Biophys J 92, 502-516.

Smaby, J.M., Brockman, H.L., 1990. Surface dipole moments of lipids at the argon-water interface. Similarities among glycerol-ester-based lipids. Biophys J 58, 195-204.

Sot, J., Goni, F.M., Alonso, A., 2005. Molecular associations and surface-active properties of short- and long-N-acyl chain ceramides. Biochim Biophys Acta 1711, 12-19.

Staneva, G., Momchilova, A., Wolf, C., Quinn, P.J., Koumanov, K., 2009. Membrane microdomains: role of ceramides in the maintenance of their structure and functions. Biochim Biophys Acta 1788, 666-675.

ten Grotenhuis, E., Demel, R.A., Ponec, M., Boer, D.R., van Miltenburg, J.C., Bouwstra, J.A., 1996. Phase behavior of stratum corneum lipids in mixed Langmuir-Blodgett monolayers. Biophys J 71, 1389-1399.

Vaknin, D., Kelley, M.S., 2000. The structure of D-erythro-C18 ceramide at the air-water interface. Biophys J 79, 2616-2623.

van Blitterswijk, W.J., van der Luit, A.H., Veldman, R.J., Verheij, M., Borst, J., 2003. Ceramide: second messenger or modulator of membrane structure and dynamics? Biochem J 369, 199-211.

Zheng, W., Kollmeyer, J., Symolon, H., Momin, A., Munter, E., Wang, E., Kelly, S., Allegood, J.C., Liu, Y., Peng, Q., Ramaraju, H., Sullards, M.C., Cabot, M., Merrill, A.H., Jr., 2006. Ceramides and other bioactive sphingolipid backbones in health and disease: lipidomic analysis, metabolism and roles in membrane structure, dynamics, signaling and autophagy. Biochim Biophys Acta 1758, 1864-1884.

Figure captions

Figure 1. C12:0 ceramide and C10:0 ceramide form ideal mixtures. A) The π-A isotherms of C10:0 Cer (uppermost), mixtures of C12:0/C10:0 Cer at 0.1 mole fraction increasing steps (from top to down) and C12:0 Cer are shown. B) Surface perpendicular dipole moment as a function of surface pressure for C10:0 Cer (open circles), mixtures with $X_{C12:0\ Cer}$ of 0.2 (filled circles), 0.4 (filled inverted triangles), 0.6 (filled squares), 0.8 (filled triangles) and C12:0 Cer (open diamonds). The arrows indicate the surface pressure at which the monolayer expanded to condensed phase transition take place. C) Surface compressibility modulus as a function of surface pressure for C10:0 Cer (open circles), mixtures with $X_{C12:0\ Cer}$ of 0.2 (filled circles), 0.4 (filled inverted triangles 0.6 (filled squares), 0.8 (filled triangles) and C12:0 Cer (open diamonds). The arrows indicate the decrease of the surface compressibility modulus that occurs during monolayer expanded to condensed transition. D) Monolayer thickness of the film $X_{C12:0\ Cer}$= 0.4 calculated by BAM as a function of surface pressure. The expanded phase (open circles) thickens at increasing values of surface pressure up to the transition surface pressure, when domains of condensed phase appear (filled circles). The variation of the thickness of a C10:0 Cer film with the surface pressure (black line) is shown for comparison.

Figure 2. A) Compositional dependence of the surface pressure at which the monolayer expanded-condensed transition occur for the mixtures C12:0 Cer/C10:0 Cer (inverted triangles); C14:0 Cer/C10:0 Cer (circles) and C24:0/C10:0 Cer (squares). B) Evolution of the size of the condensed domains on growing during monolayer compression as a function of the surface pressure for the mixtures C12:0 Cer/C10:0 Cer (inverted triangles); C14:0 Cer/C10:0 Cer (circles) and C24:0/C10:0 Cer (squares). The composition of the mixtures was X=0.4 (molar ratio of ceramide respective C10:0 Cer).

Figure 3. Mean parameters of monolayers of C12:0/C10:0 Cer mixtures at different surface pressures. Mean molecular area (A, D, G); perpendicular molecular dipole moment (B, E, H) and surface compressibility modulus (C, F, I) vs film composition are shown for the surface pressure of 3 $mN.m^{-1}$ (A, B, C); 15 $mN.m^{-1}$ (D, E, F) and 32 $mN.m^{-1}$ (G, H, I). Average values ± SEM are results of three independent experiments. Solid lines are calculated theoretical values for ideal mixing behavior.

Figure 4. Film topography of C12:0/C10:0 Cer mixtures imaged by BAM at a surface pressure of 5$mN.m^{-1}$ (A, D, G, J); 15 $mN.m^{-1}$ (B, E, H, K) and 32 $mN.m^{-1}$ (C, F, I, L). Pictures were taken during compression of the films with C12:0 Cer mole ratio of 0.2 (A, B, C); 0.4 (D, E, F); 0.6 (G, H, I) and 0.8 (J, K, L).

Figure 5. C14:0 ceramide and C10:0 ceramide form expanded mixed phases. A) The π-A isotherms of C10:0 Cer (uppermost), mixtures of C14:0/C10:0 Cer at 0.1 mole fraction increasing steps (from top to down) and C14:0 Cer are presented. The arrow at the inset shows the monolayer transition of the C10:0 Cer enriched phase for the mixtures with $X_{C14:0\ Cer}$ 0.6 to 0.9. B) Surface perpendicular dipole moment as a function of surface pressure for C10:0 Cer (open circles), mixtures with $X_{C14:0\ Cer}$ of 0.2 (filled circles), 0.4 (filled inverted triangles), 0.8 (filled triangles) and C14:0 Cer (open diamonds). The arrows indicate the surface pressure at which the monolayer expanded to condensed phase transition take place. C) Surface compressibility modulus as a function of surface pressure for C10:0 Cer (open circles), mixtures with $X_{C14:0\ Cer}$ of 0.2 (filled circles), 0.4 (filled inverted triangles), 0.6 (filled squares), 0.8 (filled triangles) and C14:0 Cer (open diamonds). The arrows indicate the decrease of the surface compressibility modulus that occurs during the monolayer expanded to condensed transition. D) Monolayer thickness of the film $X_{C14:0\ Cer}$= 0.4 calculated by BAM as a function of surface pressure. The expanded phase (open circles) thickens at increasing values of surface pressure up to the transition surface pressure, when domains of condensed phase enriched in C14:0 Cer appear (inverted filled triangles). The remaining C10:0 enriched phase does not mix in the condensed state (filled circles) with the C14:0 Cer enriched domains. The variation of the thickness of a C10:0 Cer film with the surface pressure (black line) is shown for comparison.

Figure 6. Mean parameters of monolayers of C14:0/C10:0 Cer mixtures at different surface pressures. Mean molecular area (A, D, G); perpendicular molecular dipole moment (B, E, H) and surface compressibility modulus (C, F, I) vs film composition are shown for the surface pressure of 5 $mN.m^{-1}$ (A, B, C); 15 $mN.m^{-1}$ (D, E, F) and 32 $mN.m^{-1}$ (G, H, I). Average values ± SEM are results of three independent experiments. Solid lines are calculated theoretical values for ideal mixing behavior.

Figure 7. Film topography of C14:0/C10:0 Cer mixtures imaged by BAM at a surface pressure of 5 $mN.m^{-1}$ (A, D, G, J); 15 $mN.m^{-1}$ (B, E, H, K) and 32 $mN.m^{-1}$ (C, F, I, L). Pictures were taken during compression of the films with C14:0 Cer mole ratio of 0.2 (A, B, C); 0.4 (D, E, F); 0.6 (G, H, I) and 0.8 (J, K, L).

Figure 8. C18:0 ceramide and C10:0 ceramide form phase separated films. A) The π-A isotherms of C10:0 Cer (uppermost), mixtures of C18:0/C10:0 Cer at 0.1 mole fraction increasing steps (from top to down) and C18:0 Cer are shown. B) Surface perpendicular dipole moment as a function of surface pressure for C10:0 Cer (open circles), mixtures with $X_{C18:0\ Cer}$ of 0.2 (filled circles), 0.4 (filled inverted triangles), 0.6 (filled squares), 0.8 (filled triangles) and C18:0 Cer (open diamonds). The arrows indicate the surface pressure at which the monolayer expanded to condensed phase transition take place. C) Surface compressibility modulus as a

function of surface pressure for C10:0 Cer (open circles), mixtures with $X_{C18:0\ Cer}$ of 0.2 (filled circles), 0.4 (filled inverted triangles), 0.6 (filled squares), 0.8 (filled triangles) and C18:0 Cer (open diamonds). The arrows indicate the decrease of the surface compressibility modulus during the monolayer expanded to condensed transition. D) Monolayer thickness of the film $X_{C18:0\ Cer}$= 0.4 calculated by BAM as a function of surface pressure. The expanded phase composed mainly by C10:0 Cer (open circles) thickens steadily at increasing values of surface pressure. At the transition surface pressure, a jump to higher values of thickness indicates the formation of a C10:0 Cer enriched condensed phase (filled circles). The C18:0 Cer condensed domains (inverted triangles) are formed at film spreading, and do not mix with expanded nor condensed phase of C10:0 Cer. The variation of the thickness of a C10:0 Cer film with the surface pressure (black line) is shown for comparison.

Figure 9. Mean parameters of monolayers of C18:0/C10:0 Cer mixtures at different surface pressures. Mean molecular area (A, D, G); perpendicular molecular dipole moment (B, E, H) and surface compressibility modulus (C, F, I) vs film composition are shown for the surface pressure of 5 mN.m-1 (A, B, C); 15 $mN.m^{-1}$ (D, E, F) and 32 $mN.m^{-1}$ (G, H, I). Average values ± SEM are results of three independent experiments. Solid lines are calculated theoretical values for ideal mixing behavior.

Figure 10. Film topography of C18:0/C10:0 Cer mixtures imaged by BAM at a surface pressure of 5 $mN.m^{-1}$ (A, D, G, J); 15 $mN.m^{-1}$ (B, E, H, K) and 32 $mN.m^{-1}$ (C, F, I, L). Pictures were taken during compression of the films with C18:0 Cer mole ratio of 0.2 (A, B, C); 0.4 (D, E, F); 0.6 (G, H, I) and 0.8 (J, K, L).

Figure 11. The length mismatch in the acyl chain of the N-linked fatty acid determine the mixing behavior of ceramides. The π-A isotherms of the C16:0/C12:0 mixture Cer at 40 ºC, are similar to those of the C14:0/C10:0 mixture at 24 ºC. From up and right to down and left, the C16:0 Cer content of the films are: $X_{C16:0\ Cer}$= 0; 0.1; 0.2; 0.3; 0.4; 0.6; 0.8 and 1, respectively. Inset: Transition surface pressure vs temperature of C10:0 Cer (circles), C12:0 Cer (squares), C14:0 Cer (triangles) and C16:0 Cer (diamonds). The arrows show the difference in transition surface pressure of the components of both mixtures at the respective temperatures.

Figure 12. The thickness of the expanded phase (A) and the in-plane elasticity of the films (B) for the mixtures C14:0/C10:0 Cer (squares) and C18:0/C10:0 Cer (triangles) are shown as a function of film composition. The surface pressure corresponds to 15 $mN.m^{-1}$

Figure1

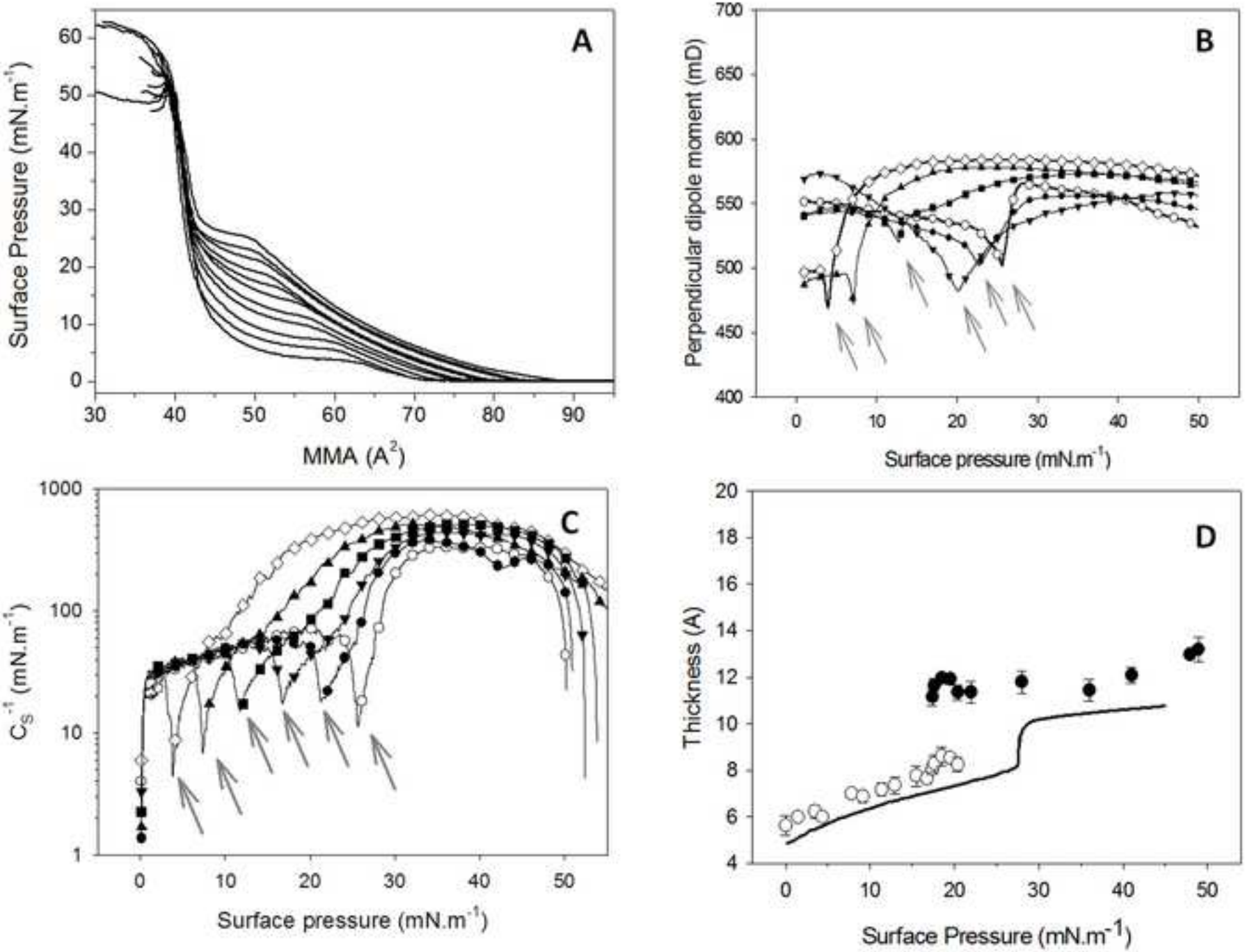
A
Surface Pressure (mN.m-1)
MMA (A2)
B
Perpendicular dipole moment (mD)
Surface pressure (mN.m-1)
C
Cs-1 (mN.m-1)
Surface pressure (mN.m-1)
D
Thickness (A)
Surface Pressure (mN.m-1)

Figure2

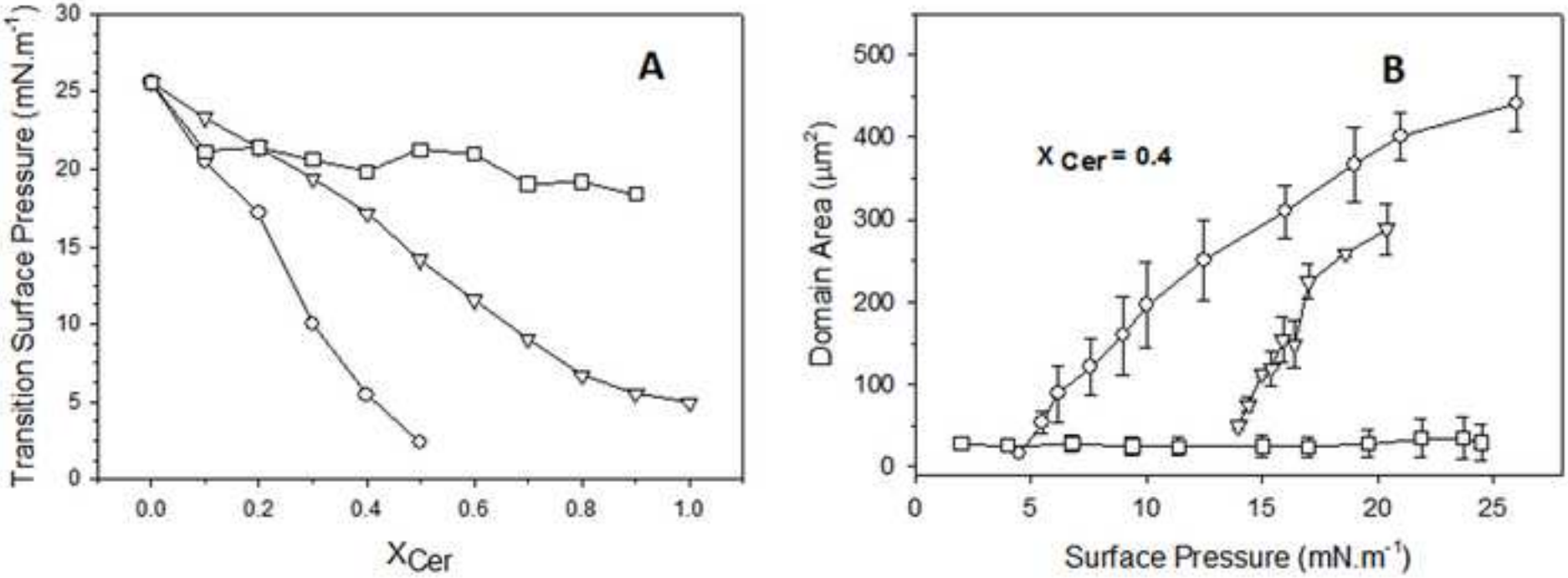
A
Transition Surface Pressure (mN.m-1)
30
25
20
15
10
5
0
0.0
0.2
0.4
0.6
0.8
1.0
XCer
B
Domain Area (µm2)
500
400
300
200
100
0
X Cer = 0.4
0
5
10
15
20
25
Surface Pressure (mN.m-1)

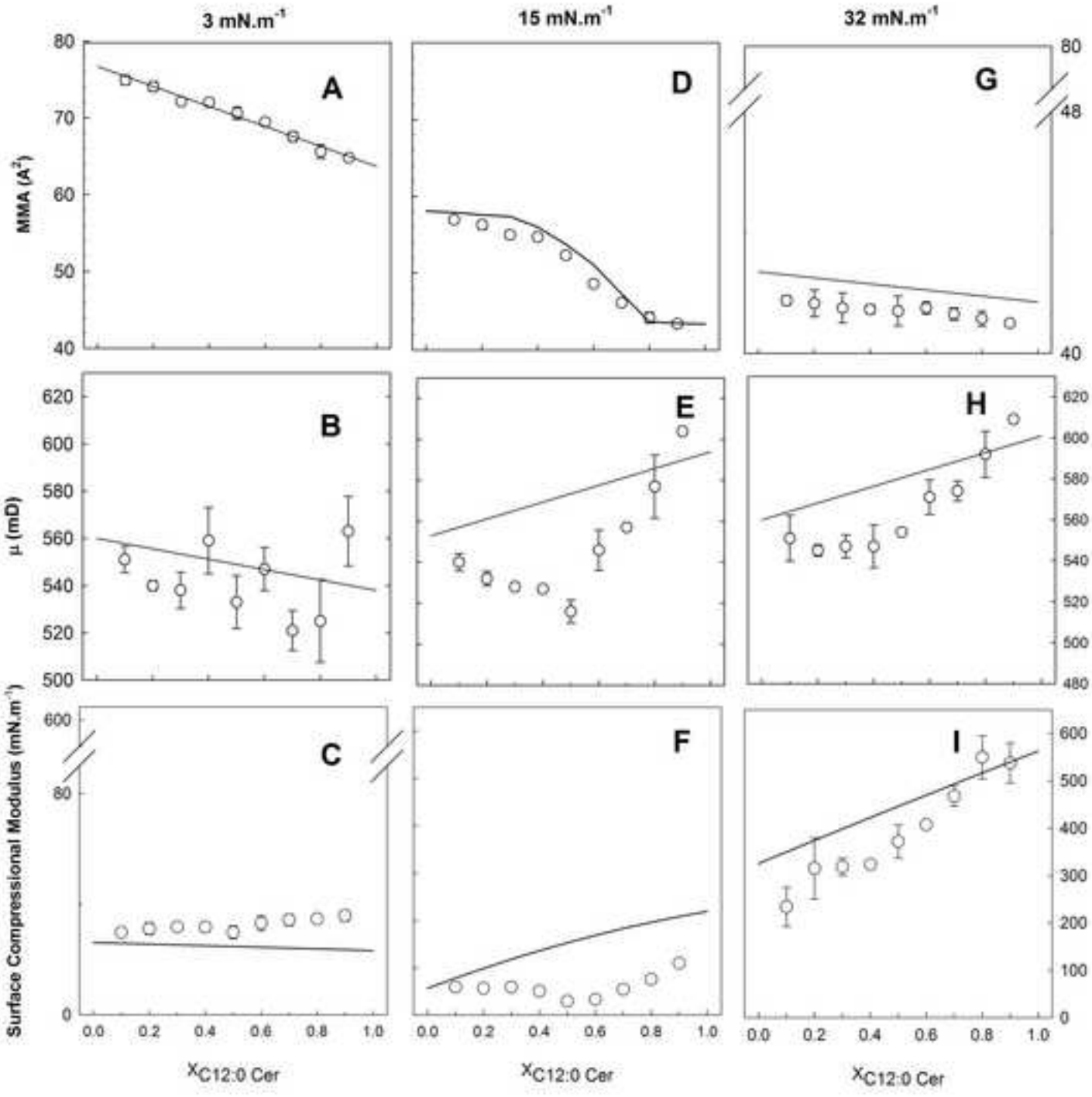

Figure4

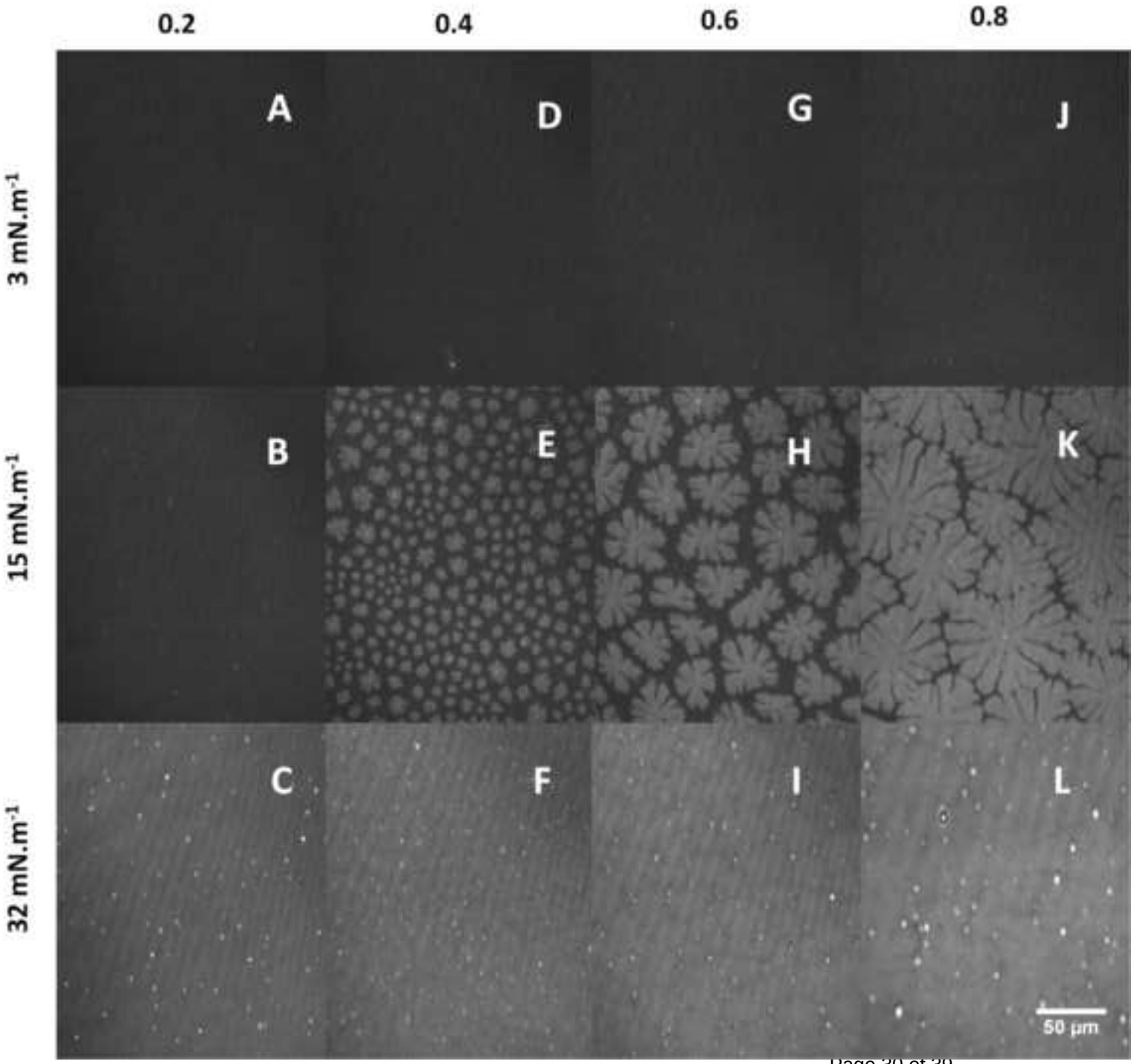

Figure5

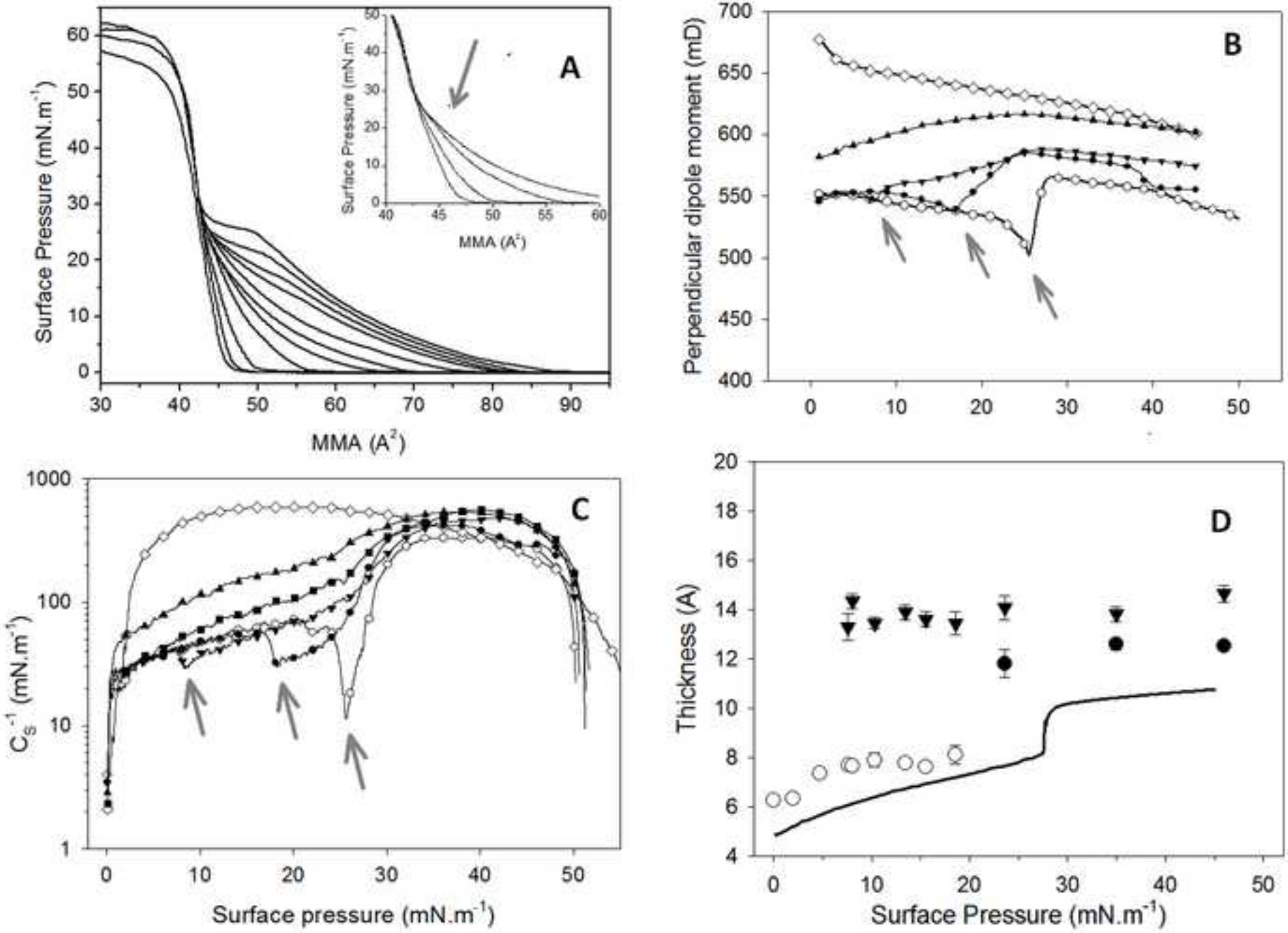
A
Surface Pressure (mN.m-1)
MMA (A2)
B
Perpendicular dipole moment (mD)
C
Cs-1 (mN.m-1)
Surface pressure (mN.m-1)
D
Thickness (A)
Surface Pressure (mN.m-1)

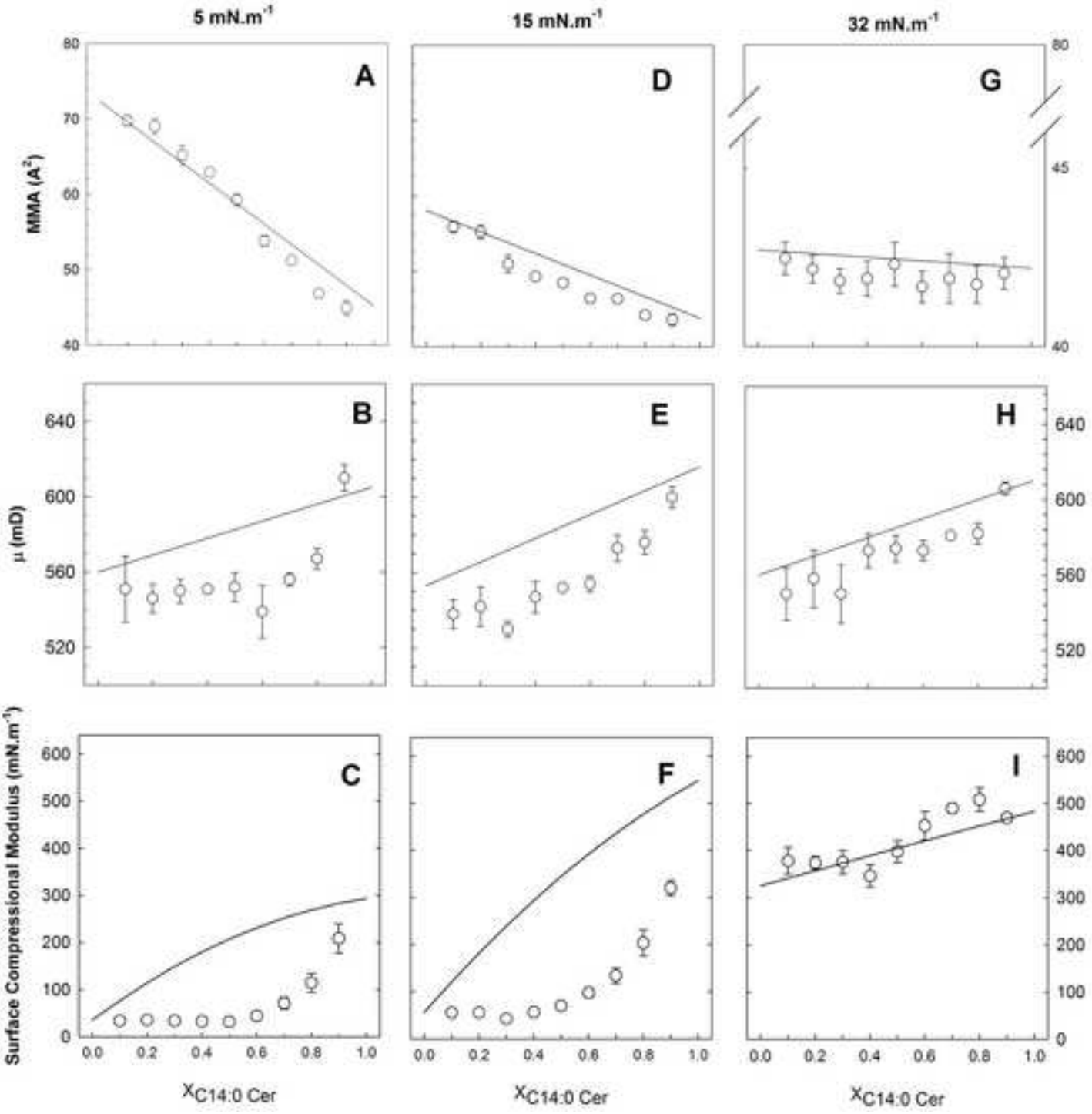

Figure7

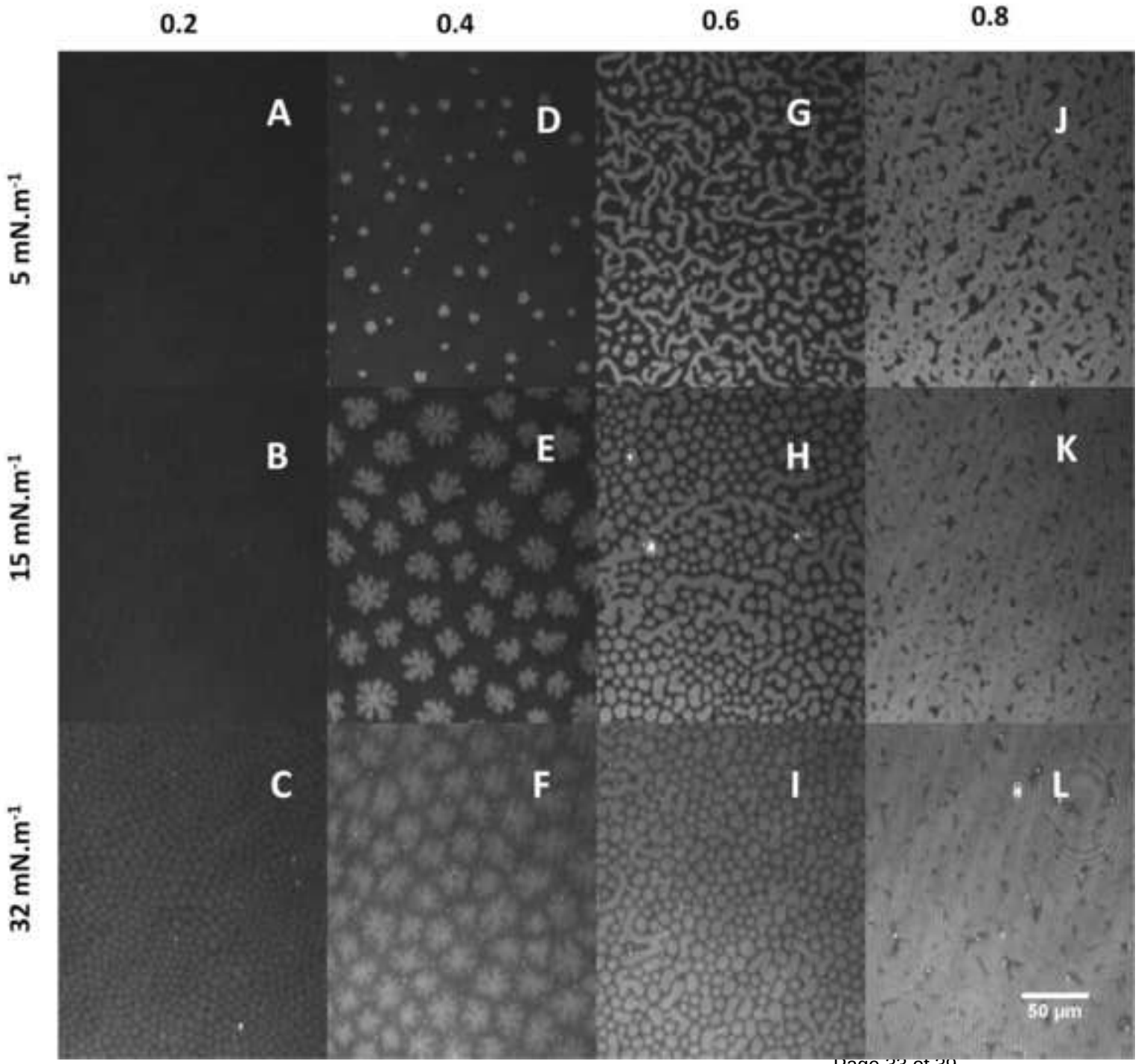

Figure8

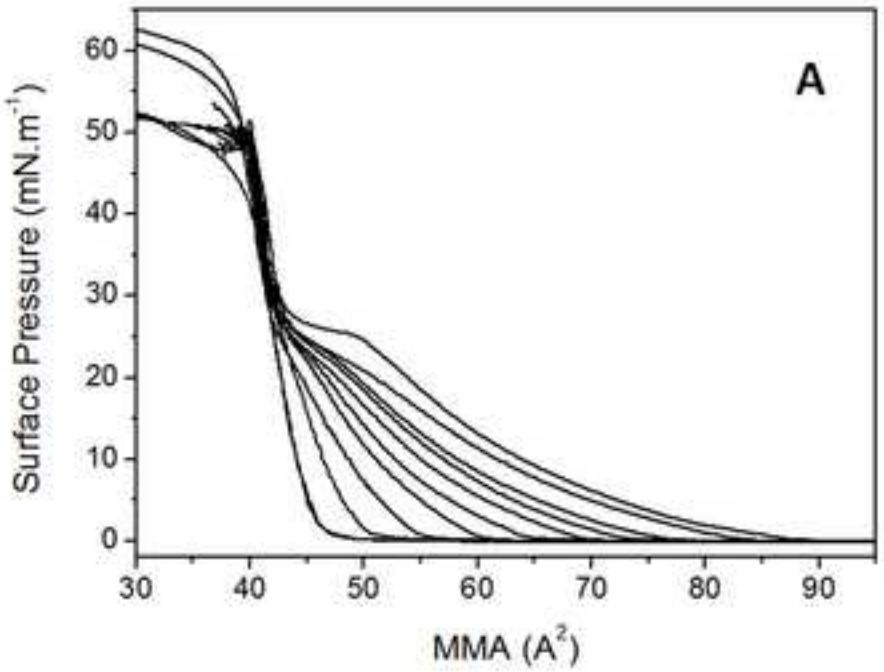
A
Surface Pressure (mN.m-1)
MMA (A2)

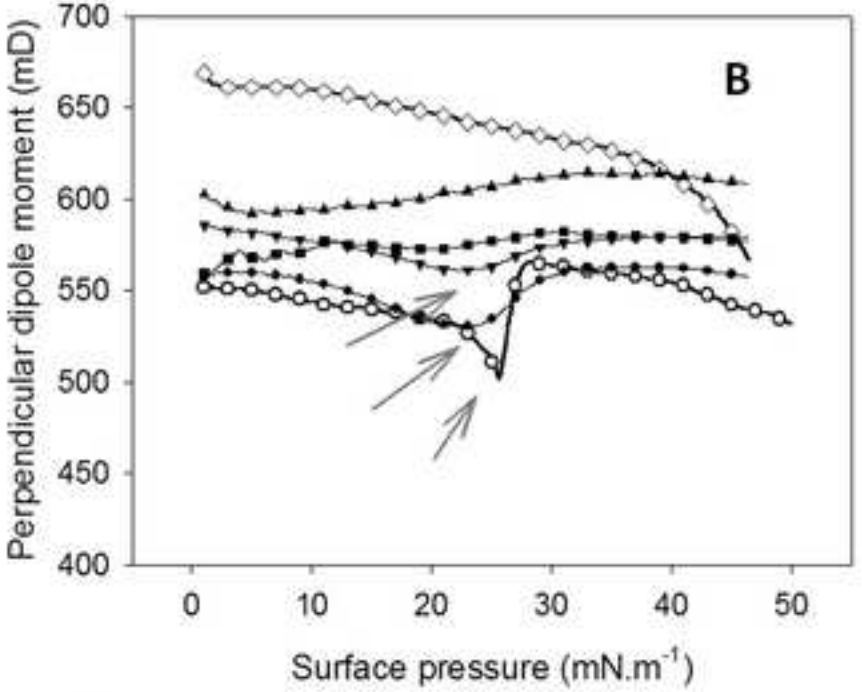
B
Perpendicular dipole moment (mD)
Surface pressure (mN.m-1)

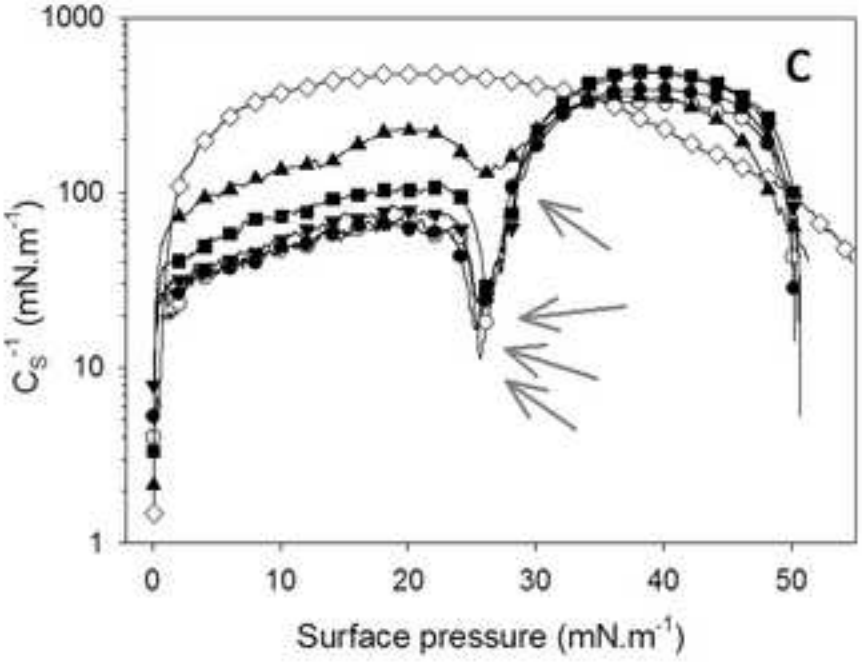
C
Cs-1 (mN.m-1)
Surface pressure (mN.m-1)

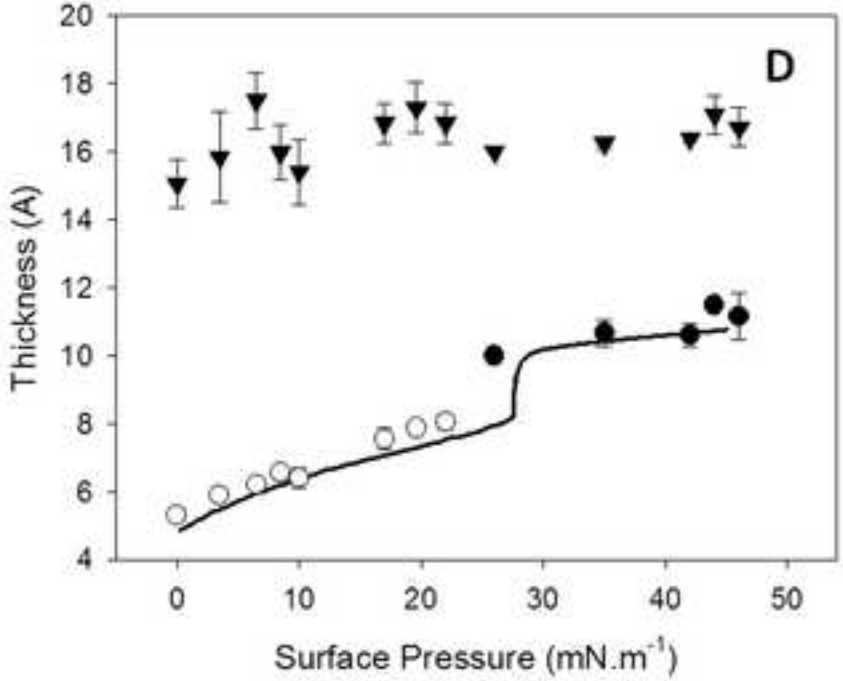
D
Thickness (A)
Surface Pressure (mN.m-1)

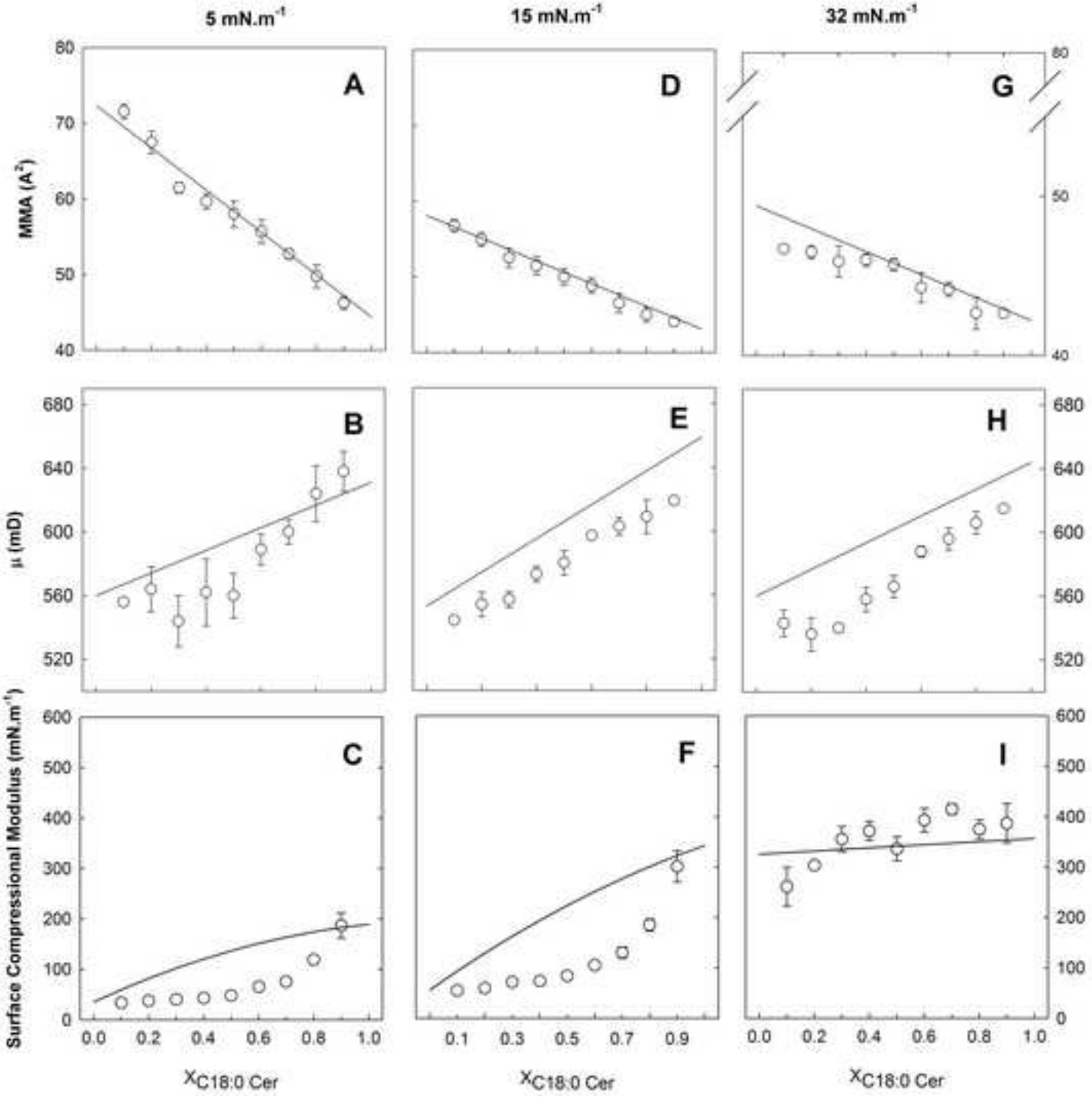

Figure10

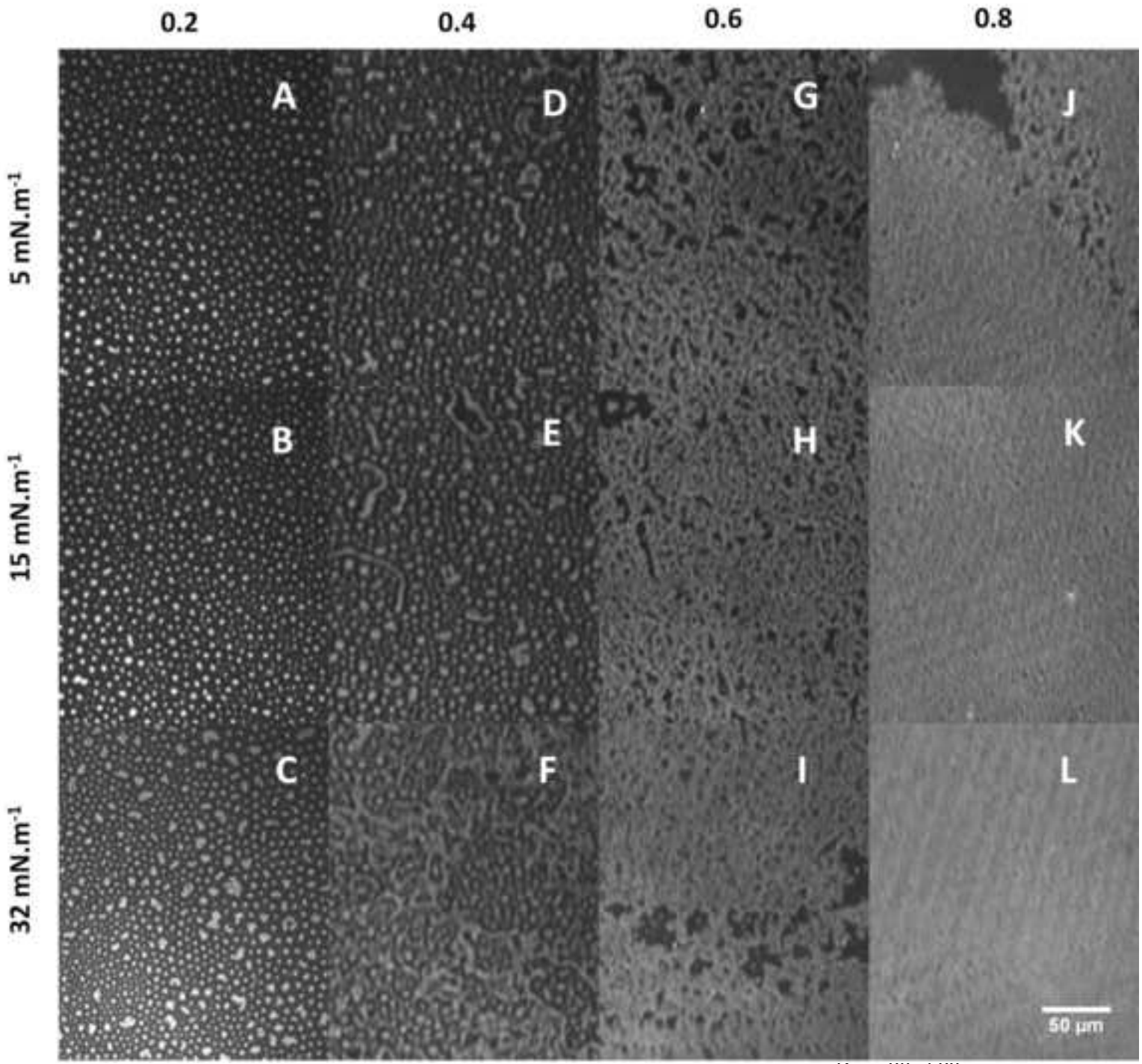

Figure11

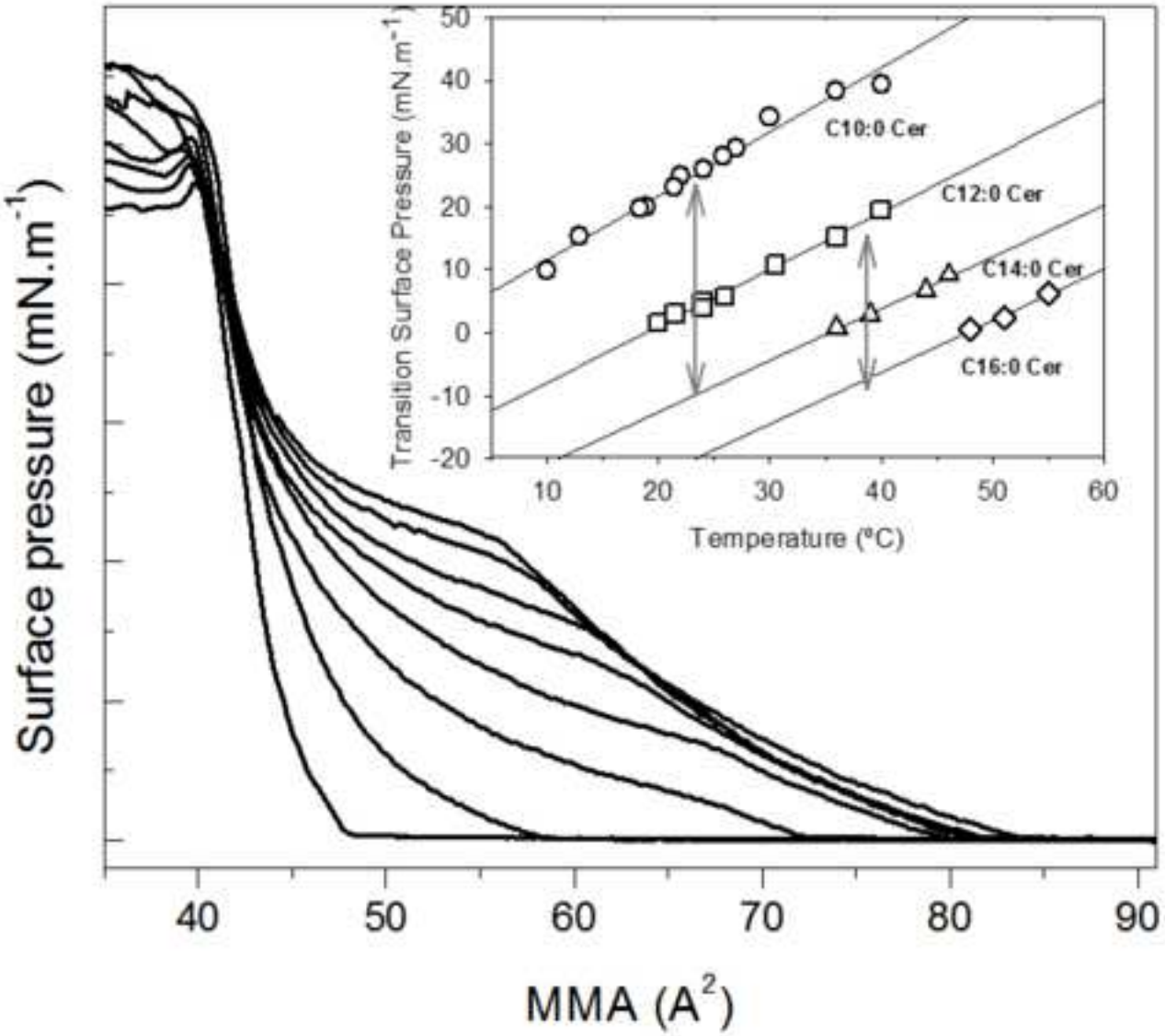
Surface pressure (mN.m-1)
MMA (A2)
40
50
60
70
80
90
Transition Surface Pressure (mN.m-1)
Temperature (ºC)
C10:0 Cer
C12:0 Cer
C14:0 Cer
C16:0 Cer
50
40
30
20
10
0
-10
-20
10
20
30
40
50
60

Figure12

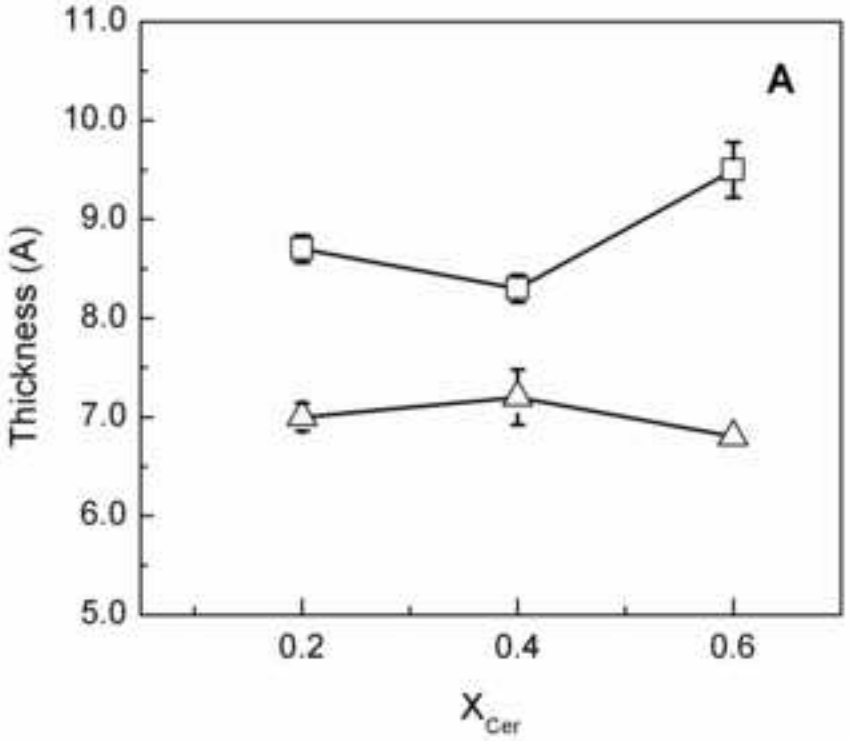
A
Thickness (A)
11.0
10.0
9.0
8.0
7.0
6.0
5.0
0.2
0.4
0.6
X Cer

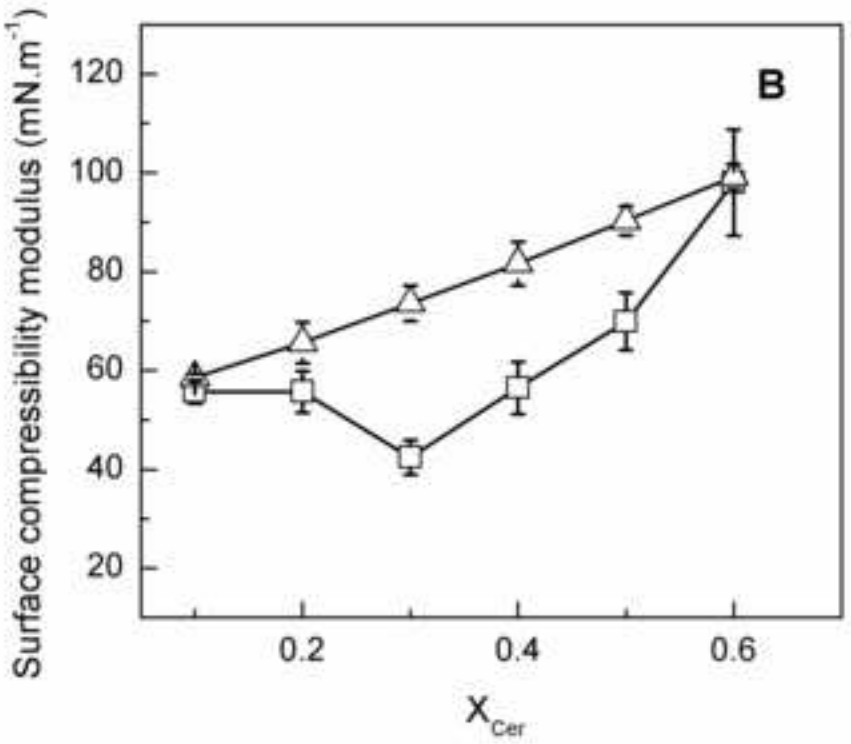
B
Surface compressibility modulus (mN.m-1)
120
100
80
60
40
20
0.2
0.4
0.6
X Cer

Highlights

Polymorphism of ceramides is determined by the N-acyl chain length.

The surface behavior of ceramide mixtures varied from ideal miscibility to total immiscibility.

The N-acyl chain length determines the ceramide mixing behavior in monolayers.